I&EC research
Industrial & Engineering Chemistry Research

Article

Cite This: Ind. Eng. Chem. Res. 2020, 59, 2275−2290

pubs.acs.org/IECR

Real-Time Adaptive Machine-Learning-Based Predictive Control of Nonlinear Processes

Zhe Wu,[†] David Rincon,[†] and Panagiotis D. Christofides*[,†,‡]

[†]Department of Chemical and Biomolecular Engineering, University of California, Los Angeles, California 90095, United States
[‡]Department of Electrical and Computer Engineering, University of California, Los Angeles, California 90095, United States

ABSTRACT: We present a machine learning-based predictive control scheme that integrates an online update of the recurrent neural network (RNN) models to capture process nonlinear dynamics in the presence of model uncertainty. Specifically, an ensemble of the RNN models are initially obtained for the nominal system, for which Lyapunov-based model predictive control (LMPC) is utilized to drive the state to the steady-state, and economic Lyapunov-based MPC (LEMPC) is applied to achieve closed-loop stability and economic optimality simultaneously. Subsequently, an event-trigger mechanism based on the decreasing rate of Lyapunov function and an error-trigger mechanism that relies on prediction errors are developed for an online model update, in which the most recent process data are utilized to derive a new ensemble of RNN models with enhanced prediction accuracy. By incorporating the event and error-triggered online RNN update within real-time machine learning-based LMPC and LEMPC, process dynamic performance is improved in terms of guaranteed closed-loop stability, optimality, and smoothness of control actions. The proposed methodology is applied to a chemical process example with time-varying disturbances under LMPC and LEMPC, respectively, to demonstrate the effectiveness of an online update of machine learning models in real-time control problems.

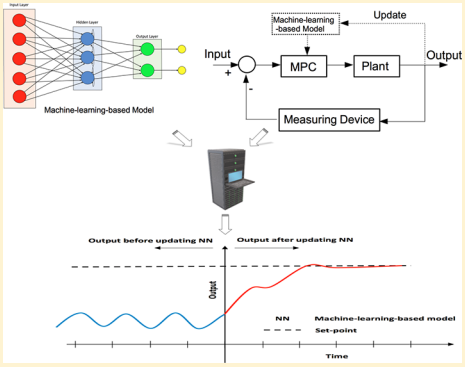

INTRODUCTION

Modeling large-scale, complex nonlinear processes has been a long-lasting challenge in process systems engineering. Model quality depends on many factors, including, but not limited to parameter estimation, model uncertainty, number of assumptions made in model development, dimensionality, model structure, and computational burden of solving the model in real-time operations.[1,2] Machine learning techniques have been successfully applied to solve regression/modeling problems based on data sets from industrial process operation or numerical simulations in process engineering, when a first-principles model is difficult to obtain. Among many machine learning methods, recurrent neural networks (RNN), a class of artificial neural network consisting of both feed-forward and feedback connections layers,[3] show promising potential for use in model-based control systems since they are capable of modeling nonlinear dynamical systems using time-series process data. In refs 4 and 5 neural networks have been applied in industrial control problems. In refs 6−8 machine learning techniques have been applied to control chemical engineering systems. In ref 9 a comparison between feed-forward neural networks and recurrent neural networks in nonlinear modeling and prediction has been discussed. Recently, RNN models have been incorporated in the design of model predictive control (MPC) systems to operate the system at its steady-state[10,11] while accounting for input and stability constraints. Additionally, based on the economic model predictive control (EMPC) that has been proposed to address process control problems accounting for process dynamics (e.g., valve actuator dynamics and actuator stiction compensation[12,13]) and dynamic economic optimization, a new class of EMPC systems that takes advantage of RNN models to predict future states has been developed in ref 14 to dynamically optimize process operating profit and achieve closed-loop stability. Although pretrained machine learning models have demonstrated to be good replacements for first-principles models in model-based controllers, a potential problem for the real-time implementation of controllers in practice is model uncertainty, which includes intrinsic and exogenous uncertaint.[15,16]

Since in real life, processes models change in time due to varying process parameters from external (e.g., aging equipment, disturbance, and new implemented technology in the process) and internal factors (e.g., fouling in the equipment), the machine learning model that has been trained using the information from past normal operations may not be able to correctly predict process states after disturbances appear. Some efforts have been made to circumvent model uncertainty using adaptive, robust, and event-triggered control within classical (first-principles) modeling and data-driven modeling techniques (e.g., neural network). For example, in the adaptive control area, a

Special Issue: Christos Georgakis Festschrift

Received: June 5, 2019
Revised: July 15, 2019
Accepted: July 24, 2019
Published: July 24, 2019

DOI: 10.1021/acs.iecr.9b03055
Ind. Eng. Chem. Res. 2020, 59, 2275−2290

methodology was proposed for high-dimensional nonlinear systems using neural networks under a triangular structure in the control inputs in which stability is guaranteed[17]. Similarly, the stability of an adaptive neural control system for two types of model uncertainty of multi-input/multi-output nonlinear systems is proven in block-triangular forms.[1] From a robust control point of view, an H_∞ controller was designed using a recurrent neural network for compensating parameter variations and external disturbances.[18] However, the above methodologies have limitations. They are only applicable to systems in which the affected parameter is known a priori and a predefined structure is needed for the inputs and the states. Additionally, in refs 19−22 the effects of model uncertainty were discussed, and data-driven models were developed to account for process uncertainty.

Considering the need to update process models as time evolves, online learning of process models using most recent process data may provide a solution to deal with model uncertainty. For example, in ref 23, a multistage online learning process was proposed using a hybrid neural network model for a real-time control of traffic signals to account for the variation of traffic volume. In ref 24 the error-triggered model reidentification has been utilized to update the process model in EMPC when the error between predicted states and measured states exceeds a threshold. It is noted that the event-triggered mechanism is able to reduce the frequency of the online update and adjustment of process models and control actions,[25,26] and thus, improve applicability and efficiency of real-time control. For example, in ref 27 an event-based control was proposed to update the actuators only when a certain threshold is violated. In ref 26 an event-triggered mechanism was proposed to stabilize the system with control actions being updated when a violation of a stability event is triggered. Additionally, the even-triggered concept has also been adopted in neural network-based control to reduce the network source utilization.[28,29] At this stage, the integration of the online update of the RNN models with the proposed MPC and EMPC using an ensemble of RNN models in refs 10 and 14 remains an open issue.

Motivated by the above, in this work, we propose real-time machine learning-based MPC and EMPC schemes that trigger an online learning of the RNN models when a threshold is violated due to unknown disturbances. Specifically, an ensemble of RNN models is initially obtained for the Lyapunov-based MPC (LMPC) and Lyapunov-based EMPC (LEMPC) to stabilize the system under normal operation (i.e., without disturbances). In the presence of time-varying disturbances, an event-triggered mechanism based on the decreasing rate of Lyapunov function and an error-triggered mechanism based on the prediction errors are developed to update RNN models during the operation using the most recent process data. Closed-loop stability analysis is performed for both LMPC and LEMPC with the online RNN model update.

The rest of this paper is organized as follows: in Preliminaries, the notations, the class of nonlinear systems considered, and the stabilizability assumptions are given. In the section "Lyapunov-Based MPC Using Ensemble of RNN Models", the general structure of the recurrent neural network and the learning algorithm are introduced. Then, a brief recap of the Lyapunov-based MPC and Lyapunov-based economic MPC using an ensemble of RNN models are provided. In the section "Event-Triggered On-Line Learning of RNNs", the event-triggered and error-triggered online RNN learning mechanisms are developed. In "Integration of On-Line Update of RNNs with MPC", the implementation strategies of online RNN learning mechanisms within LMPC and LEMPC, respectively, are presented with guaranteed closed-loop stability for both cases. In the last section, the proposed LMPC and LEMPC with the online update of the RNN models are applied to a nonlinear chemical process example to demonstrate their effectiveness.

PRELIMINARIES

Notation. The notation $|\cdot|$ is used to denote the Euclidean norm of a vector. x^T denotes the transpose of x. The notation $L_f V(x)$ denotes the standard Lie derivative $L_f V(x) := \frac{\partial V(x)}{\partial x} f(x)$ Set subtraction is denoted by "\", that is, $A\backslash B := \{x \in \mathbf{R}^n \mid x \in A, x \notin B\}$. $\mathbb{Z}^+$ denotes the set of positive integers. $\varnothing$ signifies the null set. The function $f(\cdot)$ is of class C^1 if it is continuously differentiable in its domain. A continuous function $\alpha: [0, a) \to [0, \infty)$ is said to belong to class $\mathcal{K}$ if it is strictly increasing and is zero only when evaluated at zero.

Class of Systems. The class of continuous-time nonlinear systems considered is described by the following system of first-order nonlinear ordinary differential equations:

$$\dot{x} = F(x, u, w) := f(x) + g(x)u + h(x)w, x(t_0) = x_0 \tag{1}$$

where $x \in \mathbf{R}^n$ is the state vector, $u \in \mathbf{R}^m$ is the manipulated input vector, and $w \in W$ is the disturbance vector with $W := \{w \in \mathbf{R}^q | |w| \le w_m, w_m \ge 0\}$. The control actions are constrained by $u \in U := \{u_i^{\min} \le u_i \le u_i^{\max}, i = 1, ..., m\} \subset \mathbf{R}^m$. $f(\cdot)$, $g(\cdot)$, and $h(\cdot)$ are sufficiently smooth vector and matrix functions of dimensions $n \times 1$, $n \times m$, and $n \times q$, respectively. Throughout the manuscript, we assume that the initial time t_0 is zero ($t_0 = 0$), and $f(0) = 0$ such that the origin is a steady-state of the nominal (i.e., $w(t) \equiv 0$) system of eq 1 (i.e., $(x_s^*, u_s^*) = (0,0)$, where x_s^* and u_s^* represent the steady-state state and input vectors, respectively).

Stabilization via Control Lyapunov Function. To guarantee that the closed-loop system can be stabilized, a stabilizing control law $u = \Phi(x) \in U$ that renders the origin of the nominal system of eq 1 (i.e., $w(t) \equiv 0$) exponentially stable is assumed to exist. Following converse theorems,[30] there exists a C^1 Control Lyapunov function $V(x)$ such that the following inequalities hold for all x in an open neighborhood D around the origin:

$$c_1 |x|^2 \le V(x) \le c_2 |x|^2, \tag{2a}$$

$$\frac{\partial V(x)}{\partial x} F(x, \Phi(x), 0) \le -c_3 |x|^2, \tag{2b}$$

$$\left| \frac{\partial V(x)}{\partial x} \right| \le c_4 |x| \tag{2c}$$

where c_1, c_2, c_3, and c_4 are positive constants. $F(x, u, w)$ represents the nonlinear system of eq 1. The universal Sontag control law[31] is a candidate controller for $u = \Phi(x)$.

We first characterize a region where the time-derivative of V is rendered negative under the controller $u = \Phi(x) \in U$ as follows:

$$\phi_u = \{x \in \mathbf{R}^n \mid \dot{V}(x) = L_f V + L_g V u < -k|x|^2, \; u = \Phi(x) \in U\} \cup \{0\} \tag{3}$$

where k is a positive real number. Then a level set of the Lyapunov function inside ϕ_u is used as the closed-loop stability region Ω_ρ for the nonlinear system of eq 1 as follows: $\Omega_\rho := \{x \in$

DOI: 10.1021/acs.iecr.9b03055
Ind. Eng. Chem. Res. 2020, 59, 2275−2290

$\phi_u \mid V(x) \le \rho\}$, where $\rho > 0$ and $\Omega_\rho \subset \phi_u$. From the Lipschitz property of $F(x, u, w)$ and the bounds on u and w, it follows that there exist positive constants M, L_x, L_w, L'_x, L'_w such that the following inequalities hold for all $x, x' \in D$, $u \in U$, and $w \in W$:

$$|F(x, u, w)| \le M \tag{4a}$$

$$|F(x, u, w) - F(x', u, 0)| \le L_x|x - x'| + L_w|w| \tag{4b}$$

$$\left|\frac{\partial V(x)}{\partial x}F(x, u, w) - \frac{\partial V(x')}{\partial x}F(x', u, 0)\right| \le L'_x|x - x'| + L'_w|w| \tag{4c}$$

LYAPUNOV-BASED MPC USING ENSEMBLE RNN MODELS

In this section, the structure of a recurrent neural network (RNN) model and the formulation of the Lyapunov-based MPC (LMPC) and Lyapunov-based economic MPC (LEMPC) using the RNN model ensemble to predict future states are presented. Specifically, an RNN model is first developed to approximate the nonlinear dynamics of the system of eq 1 in the operating region Ω_ρ using data from extensive open-loop simulations. Subsequently, LMPC and LEMPC are developed using an ensemble of RNN models to derive closed-loop stability for the nonlinear system of eq 1.

Recurrent Neural Network. The recurrent neural network model is developed with the following form:

$$\dot{\hat{x}} = F_{nn}(\hat{x}, u) := A\hat{x} + \Theta^{\mathrm{T}}y \tag{5}$$

where $\hat{x} \in \mathbf{R}^n$ is the RNN state vector and $u \in \mathbf{R}^m$ is the manipulated input vector. $y = [y_1, ..., y_n, y_{n+1}, ..., y_{m+n}] = [\sigma(\hat{x}_1), ..., \sigma(\hat{x}_n), u_1, ..., u_m] \in \mathbf{R}^{n+m}$ is a vector of both the network state $\hat{x}$ and the input u, where $\sigma(\cdot)$ is the nonlinear activation function (e.g., a sigmoid function $\sigma(x) = 1/(1 + e^{-x})$). A is a diagonal coefficient matrix; that is, $A = diag\{-a_1, ..., -a_n\} \in \mathbf{R}^{n \times n}$, $a_i > 0$, and $\Theta = [\theta_1, ..., \theta_n] \in \mathbf{R}^{(m+n) \times n}$ with $\theta_i = b_i[w_{i1}, ..., w_{i(m+n)}]$, where b_i, $i = 1, ..., n$ are constants. w_{ij} is the weight connecting the jth input to the ith neuron where $i = 1, ..., n$ and $j = 1, ..., (m + n)$. Throughout the manuscript, we use x to represent the state of the actual nonlinear system of eq 1 and use $\hat{x}$ for the state of the RNN model of eq 5.

The RNN model is trained following the learning algorithm in ref 14 to obtain the optimal weight vector θ_i^* by minimizing the following loss function:

$$\theta_i^* := \arg\min_{|\theta_i| \le \theta_m} \left\{ \sum_{k=1}^{N_d} |F_i(x_k, u_k, 0) + a_i x_k - \theta_i^{\mathrm{T}} y_k| \right\} \tag{6}$$

where N_d is the number of data samples used for training. To further improve the prediction accuracy of the RNN model, ensemble learning that combines multiple machine learning models is utilized to obtain the final predicted results. Specifically, following the method in ref 14, k different RNN models $F_{nn,i}(x, u)$, $i = 1, ..., k$, are trained via a k-fold cross-validation to approximate the same nonlinear system. The averaged results are calculated as the final output of the ensemble of multiple RNN models.

Lyapunov-Based Control Using an Ensemble of RNN Models. In this work, the RNN model of eq 5 is updated to capture nonlinear dynamics of the nonlinear system of eq 1 subject to time-varying bounded disturbances (i.e., $|w(t)| \le w_m$). $F^i_{nn}(x, u)$ is used to denote the ith RNN model ($i = 1, 2, ..., N_T$) that is updated using the real-time data of closed-loop state trajectories and control actions, where N_T is the total number of RNN models obtained. We assume that a set of stabilizing feedback controllers $u = \Phi^i_{nn}(x) \in U$ that can render the origin of the RNN models $F^i_{nn}(x, u)$, $i = 1,2, ..., N_T$ of eq 5 exponentially stable in an open neighborhood $\hat{D}$ around the origin exists. Therefore, there exists a C^1 Control Lyapunov function $\hat{V}(x)$ such that the following inequalities hold for all x in $\hat{D}$:

$$\hat{c}^i_1|x|^2 \le \hat{V}(x) \le \hat{c}^i_2|x|^2 \tag{7a}$$

$$\frac{\partial \hat{V}(x)}{\partial x}F^i_{nn}(x, \Phi^i_{nn}(x)) \le -\hat{c}^i_3|x|^2 \tag{7b}$$

$$\left|\frac{\partial \hat{V}(x)}{\partial x}\right| \le \hat{c}^i_4|x| \tag{7c}$$

where $\hat{c}^i_1$, $\hat{c}^i_2$, $\hat{c}^i_3$, and $\hat{c}^i_4$ are positive constants, $i = 1, 2, ..., N_T$. For the sake of simplicity, we will use symbols without the superscript of i for all the RNN models and controllers that satisfy eq 7 in the following texts. Similar to the characterization method of the closed-loop stability region Ω_ρ for the nonlinear system of eq 1, we first characterize a region

$$\hat{\phi}_u = \{x \in \mathbf{R}^n \mid \dot{\hat{V}}(x) < -\hat{c}_3|x|^2, u = \Phi_{mn}(x) \in U\} \cup \{0\}$$

from which the origin of the RNN model of eq 5 can be rendered exponentially stable under the controller $u = \Phi_{nn}(x) \in U$.

The closed-loop stability region for the RNN model of eq 5 is defined as a level set of Lyapunov functions inside $\hat{\phi}_u$: $\Omega_{\hat{\rho}} := \{x \in \hat{\phi}_u \mid \hat{V}(x) \le \hat{\rho}\}$, where $\hat{\rho} > 0$. It is noted that $\Omega_{\hat{\rho}} \subseteq \Omega_\rho$ since the data set for developing the RNN model of eq 5 is generated from open-loop simulations for $x \in \Omega_\rho$ and $u \in U$. Additionally, there exist positive constants M_{nn} and L_{nn} such that the following inequalities hold for all $x, x' \in \Omega_{\hat{\rho}}$ and $u \in U$:

$$|F_{nn}(x, u)| \le M_{nn} \tag{8a}$$

$$\left|\frac{\partial \hat{V}(x)}{\partial x}F_{nn}(x, u) - \frac{\partial \hat{V}(x')}{\partial x}F_{nn}(x', u)\right| \le L_{nn}|x - x'| \tag{8b}$$

Consider that there exists a bounded modeling error between the nominal system of eq 1 and the RNN model of eq 5 (i.e., $|\nu| = |F(x, u,0) - F_{nn}(x, u)| \le \nu_m, \nu_m > 0$), the following proposition demonstrates that the feedback controller $u = \Phi_{nn}(x) \in U$ is able to stabilize the nominal system of eq 1 if the modeling error is sufficiently small.

Proposition 1 (ref 10). Under the assumption that the origin of the closed-loop RNN system of eq 5 is rendered exponentially stable under the controller $u = \Phi_{nn}(x) \in U$ for all $x \in \Omega_{\hat{\rho}}$, if there exists a positive real number $\gamma < \hat{c}_3/\hat{c}_4$ that constrains the modeling error $|\nu| = |F(x, u,0) - F_{nn}(x, u)| \le \gamma|x| \le \nu_m$ for all $x \in \Omega_{\hat{\rho}}$ and $u \in U$, then the origin of the nominal closed-loop system of eq 1 under $u = \Phi_{nn}(x) \in U$ is also exponentially stable for all $x \in \Omega_{\hat{\rho}}$.

LMPC Using an Ensemble of RNN Models. The formulation of the LMPC using an ensemble of RNN models is given as follows:[10]

$$\mathcal{J} = \min_{u \in S(\Delta)} \int_{t_k}^{t_{k+N}} L(\tilde{x}(t), u(t))\, dt \tag{9a}$$

DOI: 10.1021/acs.iecr.9b03055
Ind. Eng. Chem. Res. 2020, 59, 2275−2290

$$\text{s.t.} \quad \dot{\tilde{x}}(t) = \frac{1}{N_e}\sum_{j=1}^{N_e} F_{nn,j}(\tilde{x}(t), u(t)) \tag{9b}$$

$$u(t) \in U, \forall\, t \in [t_k, t_{k+N}) \tag{9c}$$

$$\tilde{x}(t_k) = x(t_k) \tag{9d}$$

$$\dot{\hat{V}}(x(t_k), u) \le \dot{\hat{V}}(x(t_k), \Phi_{nn}(x(t_k))), \quad \text{if } x(t_k) \in \Omega_{\hat{\rho}} \backslash \Omega_{\rho_{nn}} \tag{9e}$$

$$\hat{V}(\tilde{x}(t)) \le \rho_{nn}, \forall\, t \in [t_k, t_{k+N}), \quad \text{if } x(t_k) \in \Omega_{\rho_{nn}} \tag{9f}$$

where $\tilde{x}$ is the predicted state trajectory, $S(\Delta)$ is the set of piecewise constant functions with period Δ, N is the number of sampling periods in the prediction horizon, and N_e is the number of regression models used for prediction. $\dot{\hat{V}}(x, u)$ is used to represent $\frac{\partial \hat{V}(x)}{\partial x}(F_{nn}(x, u))$. The optimal input trajectory computed by the LMPC is denoted by $u^*(t)$, which is calculated over the entire prediction horizon $t \in [t_k, t_{k+N})$. The control action computed for the first sampling period of the prediction horizon $u^*(t_k)$ is sent by the LMPC to be applied over the first sampling period, and the LMPC is resolved at the next sampling time.

In the optimization problem of eq 9, the objective function of eq. 9a is the integral of $L(\tilde{x}(t), u(t))$ over the prediction horizon. The constraint of eq 9b is the ensemble of RNN models of eq 5 (i.e., $F_{nn,j}$, $j = 1, ..., N_e$) that is used to predict the states of the closed-loop system. eqation 9c defines the input constraints applied over the entire prediction horizon. eqation 9d defines the initial condition $\tilde{x}(t_k)$ of eq 9b, which is the state measurement at $t = t_k$. The constraint of eq 9e forces the closed-loop state to move toward the origin if $x(t_k) \in \Omega_{\hat{\rho}} \backslash \Omega_{\rho_{nn}}$. However, if $x(t_k)$ enters $\Omega_{\rho_{nn}}$, the states predicted by the RNN model of eq 9b will be maintained in $\Omega_{\rho_{nn}}$ for the entire prediction horizon.

Based on the LMPC of eq 9, the following theorem is established to demonstrate that the LMPC optimization problem can be solved with recursive feasibility, and closed-loop stability of the nonlinear system of eq 1 is guaranteed under the sample-and-hold implementation of the optimal control actions calculated by LMPC.

Theorem 1. Consider the nominal closed-loop system of eq 1 (i.e., $w(t) \equiv 0$) under the LMPC of eq 9 based on the RNN model of eq 5 that satisfies $\gamma < \hat{c}_3/\hat{c}_4$ and the controller $\Phi_{nn}(x)$ that satisfies eq 7. Let $\Delta > 0$, $\varepsilon_w > 0$, and $\hat{\rho} > \rho_{\min} > \rho_{nn} > \rho_s$ satisfy the following inequalities:

$$-\frac{\tilde{c}_3}{\hat{c}_2}\rho_s + L_x' M \Delta \le -\varepsilon_w \tag{10}$$

and

$$\rho_{nn} := \max\{\hat{V}(\hat{x}(t+\Delta)) | \hat{x}(t) \in \Omega_{\rho_s}, u \in U\} \tag{11a}$$

$$\rho_{\min} \ge \rho_{nn} + \frac{\hat{c}_4\sqrt{\hat{\rho}}}{\sqrt{\hat{c}_1}} f_w(\Delta) + \kappa(f_w(\Delta))^2 \tag{11b}$$

where $\tilde{c}_3 = -\hat{c}_3 + \hat{c}_4\gamma > 0$ and $f_w(t) := \frac{\nu_m}{L_x}(e^{L_x t} - 1)$. Then, given any initial state $x_0 \in \Omega_{\hat{\rho}}$, there always exists a feasible solution for the optimization problem of eq 9. Additionally, it is guaranteed that under the LMPC of eq 9, $x(t) \in \Omega_{\hat{\rho}}$, $\forall\, t \ge 0$, and $x(t)$ ultimately converges to $\Omega_{\rho_{\min}}$ for the nominal closed-loop system of eq 1.

Proof. The proof of Theorem 1 can be found in ref 10.

LEMPC Using an Ensemble of RNN Models. The Lyapunov-based economic MPC (LEMPC) using an ensemble of RNN models is developed to dynamically optimize process economic benefits while maintaining the closed-loop state in the stability region for all times.[14] The LEMPC is represented by the following optimization problem:

$$\mathcal{J} = \max_{u \in S(\Delta)} \int_{t_k}^{t_{k+N}} l_e(\tilde{x}(t), u(t))\, dt \tag{12a}$$

$$\text{s.t.} \quad \dot{\tilde{x}}(t) = \frac{1}{N_e}\sum_{j=1}^{N_e} F_{nn,j}(\tilde{x}(t), u(t)) \tag{12b}$$

$$u(t) \in U, \forall\, t \in [t_k, t_{k+N}) \tag{12c}$$

$$\tilde{x}(t_k) = x(t_k) \tag{12d}$$

$$\hat{V}(\tilde{x}(t)) \le \hat{\rho}_e, \forall\, t \in [t_k, t_{k+N}), \quad \text{if } x(t_k) \in \Omega_{\hat{\rho}_e} \tag{12e}$$

$$\dot{\hat{V}}(x(t_k), u) \le \dot{\hat{V}}(x(t_k), \Phi_{nn}(x(t_k))), \quad \text{if } x(t_k) \in \Omega_{\hat{\rho}} \backslash \Omega_{\hat{\rho}_e} \tag{12f}$$

where the notations of eq 12 follow those of eq 9. The optimization problem of eq 12 optimizes the time integral of the stage cost function $l_e(\tilde{x}(t), u(t))$ of eq 12a over the prediction horizon. The prediction model of eq 12b and the initial condition of eq 12d are the same as those in the LMPC of eq 9. The constraint of eq 12e maintains the predicted closed-loop states in $\Omega_{\hat{\rho}_e}$ over the prediction horizon if $x(t_k)$ is inside $\Omega_{\hat{\rho}_e}$. However, if $x(t_k)$ enters $\Omega_{\hat{\rho}} \backslash \Omega_{\hat{\rho}_e}$, the contractive constraint of eq 12f drives the state toward the origin for the next sampling period such that the state will eventually enter $\Omega_{\hat{\rho}_e}$ within finite sampling periods.

Theorem 2. Consider the nominal closed-loop system of eq 1 under the LEMPC of eq 12 based on the controller $\Phi_{nn}(x)$ that satisfies eq 7. Let $\Delta > 0$, $\varepsilon_w > 0$, and $\hat{\rho} > \hat{\rho}_e > 0$ satisfy eq 10 and the following inequality:

$$\hat{\rho}_e \le \hat{\rho} - \frac{\hat{c}_4\sqrt{\hat{\rho}}}{\sqrt{\hat{c}_1}} f_w(\Delta) - \kappa(f_w(\Delta))^2 \tag{13}$$

Then, for any $x_0 \in \Omega_{\hat{\rho}}$, there always exists a feasible solution for the optimization problem of eq 12, and the closed-loop state $x(t)$ is bounded in the closed-loop stability region $\Omega_{\hat{\rho}}$, $\forall t \ge 0$.

Proof. The proof of Theorem 2 can be found in ref 14.

Remark 1. The RNN model is used in this work because it is able to model a continuous nonlinear dynamical system of eq 1, while a simpler artificial neural network (i.e., feed-forward neural network) is typically used to describe a steady-state relationship. Since LMPC and LEMPC rely on a continuous dynamic process model to predict future states, the RNN model is preferred in this study.

Remark 2. In this work, the RNN models are developed to replace the first-principles models used in MPC. It is noted that neural networks can also be applied to approximate the entire MPC.[32] The differences between the RNN model that replaces the first-principle model and the artificial neural network (ANN) that approximates the entire MPC are as follows: (1) the data set for RNN models are obtained from extensive open-

DOI: 10.1021/acs.iecr.9b03055
Ind. Eng. Chem. Res. 2020, 59, 2275−2290

loop simulations that capture process dynamics in the operating region, while the data set for the ANN that replaces MPC is developed based on closed-loop simulations under MPC. (2) Since the RNN model is derived to replace the first-principles model in the manuscript, the optimization problem of MPC still needs to be explicitly defined (e.g., objective function and constraints) and solved online. However, if the ANN is obtained to replace the entire MPC, the optimization problem of MPC is replaced by an input−output function described by an ANN. Additionally, it is noted that the obtained ANN may only work for the same MPC problem that is used to generate the closed-loop data set. Any modifications to the objective function or the constraints may lead to regeneration of the data set and retraining of neural networks. Therefore, it is more convenient to develop and incorporate RNN models in MPC due to its easily accessible open-loop data set and the freedom to make modifications in MPC formulation. However, if the computational efficiency is of significant importance, ANNs that replace the entire MPC can be regarded as a good solution to saving computation time and computing control actions for the closed-loop system.

EVENT-TRIGGERED ONLINE LEARNING OF RNNS

In this section, the LMPC of eq 9 and the LEMPC of eq 12 are applied to the nonlinear system of eq 1 subject to bounded disturbances (i.e., $|w(t)| \leq w_m$). Unlike the stability analysis performed for sufficiently small bounded disturbances in refs 10 and 14, in this work, we consider the case in which disturbances cannot be fully eliminated by the sample-and-hold implementation of LMPC and therefore, may render the closed-loop system unstable. To mitigate the impact of disturbances, RNN models are updated via online learning to capture the nonlinear dynamics of the system of eq 1 accounting for disturbances $w(t)$. In the following subsections, the triggering mechanisms for updating RNN models are introduced.

Event-Triggering Mechanism. In ref 33 event-triggered and self-triggered control systems were introduced to derive closed-loop stability for the system under the sample-and-hold implementation of a controller. Specifically, the event-triggered control system triggers an update of control actions if a triggering condition based on state measurements is violated, while in a self-triggered control system, the next update time can be obtained via predictions. In our work, an event-triggered online RNN learning is incorporated in the LMPC of eq 9 and the LEMPC of eq 12 to improve RNN prediction accuracy using previously received data of closed-loop states in the presence of bounded disturbances. The following theorem is established to demonstrate that if the online update of RNN is triggered by the violation of eq 14, the minimal interevent time $T_k = r_{k+1} - r_k$ is bounded from below, where r_k represents the kth violation of eq 14, $k \in \mathbb{Z}^+$.

Theorem 3. Consider the nonlinear system $\dot{x} = F(x, u, w)$ of eq 1 in the presence of bounded disturbances $|w(t)| \leq w_m$, and the RNN model $\dot{\hat{x}} = F_{nn}(\hat{x}, u)$ of eq 5 that has been updated at $t = t_k = r_k$ to approximate the dynamic behavior of the system of eq 1 before $t = t_k$ with a sufficiently small modeling error $|\nu| \leq \gamma |x|$, $\gamma < \hat{c}_3/\hat{c}_4$. If the stabilizing controller $u = \Phi_{nn}(x) \in U$ is implemented in a sample-and-hold fashion (i.e., $u(t) = \Phi_{nn}(\hat{x}(t_k))$, $\forall t \in [t_k, t_{k+1})$, where $t_{k+1} := t_k + \Delta$ and Δ is the sampling period), and the $k+1$th update of the RNN model is triggered at $t = r_{k+1}$ by the violation of the following inequality for all $x \in \Omega_{\hat{\rho}} \backslash \Omega_{\rho_s}$:

$$V(x(t)) \leq V(x(t_k)) - \varepsilon_w(t - t_k),\ t \in [t_k, t_{k+1}) \tag{14}$$

where $\varepsilon_w > 0$ and ρ_s satisfy eq10 and eq 11 in Theorem 1, then there exists a positive constant τ^* such that the minimal interevent time $T_k = r_{k+1} - r_k \geq \tau^*$.

Proof. Since the controller $u = \Phi_{nn}(x) \in U$ is implemented in a sample-and-hold fashion, given $x(t_k) = \hat{x}(t_k) \in \Omega_{\hat{\rho}} \backslash \Omega_{\rho_s}$, we first derive the time-derivative of $\hat{V}(x)$ for the nonlinear system of eq 1 (i.e., $\dot{x} = F(x, u, w)$) in the presence of bounded disturbances (i.e., $|w| \leq w_m$) over $t \in [t_k, t_{k+1})$ as follows:

$$\begin{aligned}
\dot{\hat{V}}(x(t)) &= \frac{\partial \hat{V}(x(t))}{\partial x} F(x(t), \Phi_{nn}(x(t_k)), w(t)) \\
&= \frac{\partial \hat{V}(x(t_k))}{\partial x} F(x(t_k), \Phi_{nn}(x(t_k)), w(t_k)) \\
&\quad + \frac{\partial \hat{V}(x(t))}{\partial x} F(x(t), \Phi_{nn}(x(t_k)), w(t)) \\
&\quad - \frac{\partial \hat{V}(x(t_k))}{\partial x} F(x(t_k), \Phi_{nn}(x(t_k)), w(t_k))
\end{aligned} \tag{15}$$

The first term

$$\frac{\partial \hat{V}(x(t_k))}{\partial x} F(x(t_k), \Phi_{nn}(x(t_k)), w(t_k))$$

in the above equation can be further expanded as follows:

$$\begin{aligned}
&\frac{\partial \hat{V}(x(t_k))}{\partial x} F(x(t_k), \Phi_{nn}(x(t_k)), w(t_k)) \\
&= \frac{\partial \hat{V}(x(t_k))}{\partial x} (F_{nn}(x, \Phi_{nn}(x(t_k))) \\
&\quad + F(x, \Phi_{nn}(x(t_k)), w(t_k)) - F_{nn}(x, \Phi_{nn}(x(t_k)))) \\
&\leq -\hat{c}_3 |x(t_k)|^2 + \hat{c}_4 |x(t_k)| (F(x(t_k), \Phi_{nn}(x(t_k)), w(t_k)) \\
&\quad - F_{nn}(x(t_k), \Phi_{nn}(x(t_k)))) \\
&\leq -\hat{c}_3 |x(t_k)|^2 + \hat{c}_4 \gamma |x(t_k)|^2 \\
&\leq -\tilde{c}_3 |x(t_k)|^2
\end{aligned} \tag{16}$$

where $\tilde{c}_3 = -\hat{c}_3 + \hat{c}_4 \gamma > 0$ is a positive real number that has been defined in Theorem 1. Specifically, the inequalities in eq 16 are derived from the fact that

$$\frac{\partial \hat{V}(x(t))}{\partial x} F_{nn}(x(t), \Phi_{nn}(x)) \leq -\hat{c}_3 |x(t)|^2$$

holds for all $x \in \Omega_{\hat{\rho}} \backslash \Omega_{\rho_s}$ and the RNN model $\dot{\hat{x}} = F_{nn}(\hat{x}, u)$ is well-trained at $t = t_k$ such that the modeling error $|\nu| = |F(x, u, w) - F_{nn}(\hat{x}, u)|$, $\forall t \in [0, t_k]$ is constrained by $|\nu| \leq \gamma |x|$. On the basis of eq16 and eq 4, the time-derivative of $\hat{V}$ in eq 15 can be simplified as follows:

$$\begin{aligned}
\dot{\hat{V}}(x(t)) &\leq -\tilde{c}_3 |x(t_k)|^2 + \frac{\partial \hat{V}(x(t))}{\partial x} F(x(t), \Phi_{nn}(x(t_k)), w(t)) \\
&\quad - \frac{\partial \hat{V}(x(t_k))}{\partial x} F(x(t_k), \Phi_{nn}(x(t_k)), w(t_k)) \\
&\leq -\tilde{c}_3 |x(t_k)|^2 + L'_x |x(t) - x(t_k)| + L'_w |w(t) - w(t_k)|
\end{aligned} \tag{17}$$

Let $p(t) = \hat{V}(x(t))$ and $q(t) = \tilde{V}(x(t)) = \hat{V}(x(t_k)) - \varepsilon_w(t - t_k)$. It is readily shown that $p(t)$ and $q(t)$ are C^1 functions and $p(t_k) = q(t_k) = \hat{V}(x(t_k))$ holds. It follows that $\dot{q}(t_k) = \dot{\tilde{V}}(x(t_k)) = -\varepsilon_w$.

DOI: 10.1021/acs.iecr.9b03055
Ind. Eng. Chem. Res. 2020, 59, 2275−2290

Additionally, using eq 2 and eq 17, $\dot{p}(t_k)$ is bounded by the following inequality:

$$\begin{aligned}\dot{p}(t_k) &= \dot{\hat{V}}(x(t_k))\\ &\le -\tilde{c}_3|x(t_k)|^2 + L_x'|x(t_k) - x(t_k)|\\ &\quad + L_w'|w(t_k) - w(t_k)|\\ &\le -\frac{\tilde{c}_3}{\hat{c}_2}\hat{V}(x(t_k))\end{aligned} \tag{18}$$

Therefore, it is derived that $\dot{p}(t_k) < \dot{q}(t_k)$ for all $x(t_k) \in \Omega_{\hat{\rho}}\backslash\Omega_{\rho_s}$ since ε_w is chosen to satisfy eq 10 (i.e., $-\frac{\tilde{c}_3}{\hat{c}_2}\rho_s + L_x'M\Delta \le -\varepsilon_w$). Following the Lemma in ref 26, it is shown that the minimal interevent time T_k satisfies $T_k \ge \tau^*$, where τ^* is the smallest positive solution to the equation $p(t) = q(t)$, due to the continuity properties of p, q, $\dot{p}$, $\dot{q}$. This completes the proof of Theorem 3.

Remark 3. Theorem 3 demonstrates that the existence of a nonzero minimal interevent time T_k is guaranteed for the nonlinear system of eq 1 subject to the triggering condition of eq 14. This implies that the above sample-and-hold implementation of the controller $u = \Phi_{nn}(x) \in U$ with the triggering condition of eq 14 can be applied in practice in which the update of RNN models cannot be triggered in a continuous-time manner.

Remark 4. Since the upper bound of the evolution of $V(x)$ given in eq 14 guarantees the decrease of $V(x)$ over time, the closed-loop state can be ultimately driven into a small neighborhood around the origin (i.e., Ω_{ρ_s}) under the controller $u = \Phi_{nn}(x) \in U$ provided that the RNN models of eq 5 and control actions are updated every time the condition of eq 14 is violated (i.e., at $t = r_k$, $k = 1, 2, ...$). However, considering the fixed sampling period Δ in the sample-and-hold implementation of the LMPC of eq 9 and the LEMPC of eq 12, control actions based on the updated RNN models will not be calculated immediately after the violation of eq 14 since the control actions remain the same during the current sampling period. For example, if the $(k+1)$th RNN update is triggered at $t = r_{k+1}$, where $r_{k+1} \in (t_k, t_{k+1})$, the control actions are calculated based on the new RNN models at the next sampling time $t = t_{k+1}$ instead of $t = r_{k+1}$. Because of the asynchronization between updating RNN models and recalculating control actions, eq 14 may not hold for all times, and thus, the closed-loop state is no longer guaranteed to move toward the origin within each sampling period. To address the above issue, an additional constraint is proposed for the sampling period in the following subsection to ensure that the closed-loop state can still be driven to a neighborhood around the origin under asynchronous updates of RNN models and control actions.

Stability Analysis of Event-Triggered Feedback Systems. Since model uncertainty (i.e., bounded disturbances $|w(t)| \le w_m$) is introduced into the nonlinear system of eq 1 under the sample-and-hold implementation of the controller $u = \Phi_{nn}(x) \in U$ that incorporates the event-triggered mechanism of eq 14, closed-loop stability derived for the nominal system of eq 1 does not hold for all x in $\Omega_{\hat{\rho}}$. In this section, we show that the controller $u = \Phi_{nn}(x) \in U$ can maintain the state inside the stability region $\Omega_{\hat{\rho}}$ for all times and ultimately drive the state into a region around the origin for the closed-loop system of eq 1 subject to bounded disturbances.

The following proposition is developed to demonstrate that if the RNN model update is triggered within a certain sampling period, yet the control actions remain unchanged till the end of this sampling period, closed-loop stability is still guaranteed in the sense that the closed-loop state moves toward the origin within one sampling period for all $x \in \Omega_{\hat{\rho}}\backslash\Omega_{\rho_w}$, where $\rho_w \ge \max_{x\in\Omega_{\hat{\rho}}}\{\hat{V}(x) \mid \dot{\hat{V}}(x) \ge -\hat{c}_3|x|^2 - 2L_w'w_m,\ u = \Phi_{nn}(x) \in U\}$. Additionally, ρ_w is designed such that if the current state is inside Ω_{ρ_w}, it will not leave $\Omega_{\hat{\rho}}$ within one sampling period.

Proposition 2. Consider the system of eq 1 with bounded disturbances (i.e., $|w(t)| \le w_m$) under the sample-and-hold implementation of the controller $u = \Phi_{nn}(x) \in U$. Let $\hat{\rho} > \rho_w > 0$ and Δ satisfy eq 10 and the following inequality:

$$\Delta < \frac{2\left(\frac{\tilde{c}_3}{\hat{c}_2}\rho_w - 2L_w'w_m\right)}{L_x'M} \tag{19}$$

Then, for any $x(t_k) \in \Omega_{\hat{\rho}}\backslash\Omega_{\rho_w}$, it holds that

$$\hat{V}(x(t)) < \hat{V}(x(t_k)),\ \forall\ t \in (t_k, t_{k+1}] \tag{20}$$

Proof. Assuming $x(t_k) \in \Omega_{\hat{\rho}}\backslash\Omega_{\rho_w}$, we prove that within one sampling period, the value of $\hat{V}(x(t))$ does not exceed that of $\hat{V}(x(t_k))$ for all $t \in [t_k, t_{k+1}]$ in the case that the RNN model updated at $t = r_k < t_k$ does not account for current disturbances $w(t)$ at all. On the basis of eq 15, the time-derivative of $\hat{V}(x)$ in the presence of disturbances is derived as follows:

$$\begin{aligned}\dot{\hat{V}}(x(t)) &= \frac{\partial\hat{V}(x(t))}{\partial x}F(x(t), \Phi_{nn}(x(t_k)), w(t))\\ &= \frac{\partial\hat{V}(x(t_k))}{\partial x}F(x(t_k), \Phi_{nn}(x(t_k)), w(r_k))\\ &\quad + \frac{\partial\hat{V}(x(t))}{\partial x}F(x(t), \Phi_{nn}(x(t_k)), w(t))\\ &\quad - \frac{\partial\hat{V}(x(t_k))}{\partial x}F(x(t_k), \Phi_{nn}(x(t_k)), w(r_k))\end{aligned} \tag{21}$$

Using the similar expansion that was performed in eq 16, we derive the following equation:

$$\begin{aligned}&\frac{\partial\hat{V}(x(t_k))}{\partial x}F(x(t_k), \Phi_{nn}(x(t_k)), w(r_k))\\ &= \frac{\partial\hat{V}(x(t_k))}{\partial x}(F_{nn}(x, \Phi_{nn}(x(t_k)))\\ &\quad + F(x, \Phi_{nn}(x(t_k)), w(r_k)) - F_{nn}(x, \Phi_{nn}(x(t_k))))\end{aligned} \tag{22}$$

Since the RNN model obtained at $t = r_k$ guarantees that the modeling error between the kth RNN model and the uncertain nonlinear system of eq 1 subject to disturbances $w(t)$, $\forall t \in [r_{k-1}, r_k]$ is sufficiently small (i.e., $|F(x, \Phi_{nn}(x), w(r_k)) - F_{nn}(x, \Phi_{nn}(x))| \le \gamma|x|$), the following inequalities can be obtained using eq 4

$$\begin{aligned}\dot{\hat{V}}(x(t)) &\le -\hat{c}_3|x(t_k)|^2 + \hat{c}_4\gamma|x(t_k)|^2 + L_x'|x(t) - x(t_k)|\\ &\quad + L_w'|w(t) - w(r_k)| \le -\tilde{c}_3|x(t_k)|^2 + L_x'|x(t) - x(t_k)|\\ &\quad + L_w'|w(t) - w(r_k)|\end{aligned} \tag{23}$$

From the above inequality, it is noted that the disturbance term $|w(t) - w(r_k)|$ could be nonzero for all $t \in [t_k, t_{k+1}]$ because the

DOI: 10.1021/acs.iecr.9b03055
Ind. Eng. Chem. Res. 2020, 59, 2275−2290

last updated RNN model (i.e., the kth RNN model obtained at $t = r_k < t_k$) does not account for time-varying disturbances over $t \in (r_k, t_k]$. Therefore, we show that eq 20 holds for all $x \in \Omega_{\hat{\rho}} \backslash \Omega_{\rho_w}$ under the worst-case scenario that $|w(t) - w(r_k)| = 2w_m, \forall t \in [t_k, t_{k+1}]$. Specifically, based on eq 21, eq 22, and the fact that

$$\frac{\partial \hat{V}(x(t_k))}{\partial x} F_{nn}(x, \Phi_{nn}(x(t_k))) < -\hat{c}_3 |x(t_k)|^2 - 2L_w' w_m$$

for all $x(t_k) \in \Omega_{\hat{\rho}} \backslash \Omega_{\rho_w}$, it is obtained that

$$\begin{aligned} \dot{\hat{V}}(x(t_k)) &\le -\hat{c}_3 |x(t_k)|^2 - 2L_w' w_m + \hat{c}_4 \gamma |x(t_k)|^2 \\ &\quad + L_x' |x(t_k) - x(t_k)| + L_w' |w(t_k) - w(r_k)| \\ &\le -\frac{\tilde{c}_3}{\hat{c}_2} \rho_w \end{aligned} \tag{24}$$

It follows that $x(t)$ initially moves toward the origin during $t \in [t_k, t_{k+1}]$ due to $\dot{\hat{V}}(x(t)) < 0$ at $t = t_k$. Next, we show that $\hat{V}(x(t)) < \hat{V}(x(t_k))$ holds for all $t \in (t_k, t_{k+1}]$ provided that the sampling period Δ is sufficiently small. From eq 4a and eq 23, it is obtained that

$$\dot{\hat{V}}(x(t)) \le -\frac{\tilde{c}_3}{\hat{c}_2} \hat{V}(x(t_k)) + L_x' M |t - t_k| + 2L_w' w_m,$$
$$\forall\, t \in [t_k, t_{k+1}]$$

Thus, the evolution of $\hat{V}(x(t))$, $t \in [t_k, t_{k+1}]$ is calculated as follows by letting $\tau = t - t_k$:

$$\hat{V}(x(t)) \le V(x(t_k)) + \left(2L_w' w_m - \frac{\tilde{c}_3}{\hat{c}_2} \rho_w\right) \tau + \frac{L_x' M}{2} \tau^2 \tag{25}$$

Therefore, if the sampling period satisfies eq 19, it is guaranteed that $\hat{V}(x(t)) < \hat{V}(x(t_k))$ for all $t \in (t_k, t_{k+1}]$, where $t_{k+1} := t_k + \Delta$. This implies that for all $x(t_k) \in \Omega_{\hat{\rho}} \backslash \Omega_{\rho_w}$, the state is bounded in $\Omega_{\hat{\rho}}$ for all times, and can be ultimately driven into Ω_{ρ_w} under $u = \Phi_{nn}(x) \in U$.

Remark 5. Although the controller $u = \Phi_{nn}(x) \in U$ is able to drive the state toward the origin for all $x \in \Omega_{\hat{\rho}} \backslash \Omega_{\rho_w}$, the rate of convergence could be slow due to the large model mismatch if the RNN models are not updated following the event-triggering mechanism of eq 14. Therefore, to accelerate convergence, it is necessary for the RNN models to be updated online to improve approximation performance. For example, the online update of the $k+1$th RNN model is triggered at $t = r_{k+1}$ to capture the dynamics of the nonlinear system of eq1 accounting for time-varying disturbances since the last update invocation (i.e., $t \in [r_k, r_{k+1}]$). As a result, the new RNN models work compatibly with the controller to stabilize the nonlinear system of eq 1 until the model mismatch increases to an undesired level and eventually leads to the next violation of eq 14.

Remark 6. Suppose that an online update of RNN models is triggered at some point within one sampling period (e.g., $r_k \in (t_k, t_{k+1})$). Since the control actions remain unchanged till the next sampling step t_{k+1} due to the sample-and-hold implementation of the controller, Proposition 2 demonstrates that for any $x(t_k) \in \Omega_{\hat{\rho}} \backslash \Omega_{\rho_w}$, the state $x(t), \forall (t_k, t_{k+1}]$ can still move toward a smaller level set of $\hat{V}(x)$ if the sampling period Δ satisfies eq 19. The above stability property facilitates and eases the incorporation of the event-triggered update of RNN models into the LMPC of eq 9 and the LEMPC of eq 12 where a fixed sampling period Δ is used.

Error-Triggered Online RNN Update. The above sections have demonstrated that the closed-loop state of the system of eq 1 subject to bounded disturbances can be driven into Ω_{ρ_w} under $u = \Phi_{nn}(x) \in U$ with the online update of the RNN models. Since $\dot{\hat{V}}(x(t))$ is no longer guaranteed to be rendered negative within one sampling period under the sample-and-hold implementation of $u = \Phi_{nn}(x) \in U$, in this section, another event-triggering mechanism based on errors between predicted states and measured states is developed to update the RNN models for all $x \in \Omega_{\rho_w}$. To differentiate it with the event-triggered mechanism developed for $x \in \Omega_{\hat{\rho}} \backslash \Omega_{\rho_w}$ in eq 14, it will be termed the error-triggered online RNN update throughout the manuscript. Specifically, following the error-triggering mechanism in ref 24 a moving horizon error metric $E_{\mathrm{rnn}}(t_k)$ is proposed to indicate the prediction accuracy of RNN models at $t = t_k$ as follows:

$$E_{\mathrm{rnn}}(t_k) = \sum_{i=0}^{N_b} \frac{|x_p(t_{k-i}) - x(t_{k-i})|}{|x(t_{k-i})| + \delta} \tag{26}$$

where N_b is the number of sampling periods before t_k that contribute to the quantification of the prediction error. $x_p(t_{k-i})$, $i = 0, \ldots, N_b$ are the predictions of the past states using RNN models, while $x(t_{k-i})$ are the past state measurements from the actual nonlinear system of eq 1 under the same control actions. A small positive real number δ is added in the denominator of eq 26 to avoid the division by small numbers when $x(t_{k-i})$ approaches zero. The RNN models are updated if the following inequality is satisfied (i.e., the accumulated error $E_{\mathrm{rnn}}(t_k)$ exceeds the threshold E_T):

$$E_{\mathrm{rnn}}(t_k) > E_T \tag{27}$$

where E_T is determined via extensive closed-loop simulations. Specifically, we first choose an appropriate length N_b for the moving horizon such that it is not too short to frequently trigger the update of RNN models, nor too long to cause data-storage burden. Subsequently, on the basis of extensive closed-loop simulations, the threshold E_T is determined off-line to trigger an RNN model update if the state error has accumulated to an undesired level. Additionally, common measurement noise (sufficiently small compared to time-varying disturbances from model uncertainty) and nonzero modeling error of RNN models should be accounted for in determining the value of E_T such that they do not trigger an update of RNN models in most times. Lastly, after the RNN model is updated, for example, at $t = r_k$, all the errors before $t = r_k$ are reset to zero.

Remark 7. To ensure that an online update of RNN models can be accomplished within one sampling period, a new ensemble of RNN models is obtained based on previous RNN models and most recent process data. Specifically, instead of training a new ensemble of RNN models from randomly initialized weights, the weights in previous RNN models are imported as the initial weight values for the updated ensemble of RNN models. Additionally, it should be noted that only the initial ensemble of RNN models (i.e., pretrained models for the nominal system of eq 1) is trained based on the entire data set from extensive open-loop simulations. All the following updated RNN models (i.e., fine-tuning of RNN models) are developed using new collected process data.

Remark 8. The online update of RNN models via the fine-tuning method (i.e., using most recent data set only) has many advantages. First, since we initialize RNN weights which are

DOI: 10.1021/acs.iecr.9b03055
Ind. Eng. Chem. Res. 2020, 59, 2275−2290

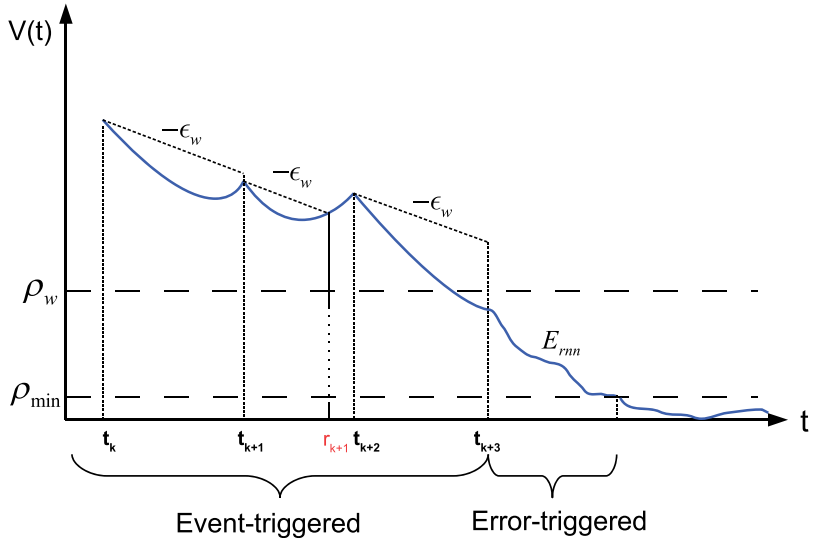

Figure 1. Evolution of Lyapunov function (blue trajectory) under the LMPC with the event-triggered condition of eq 14 and error-triggered condition of eq 27, where the dashed lines with the slope $-\varepsilon_w$ represent the threshold lines in eq 14.

obtained from previous RNN models, some of the underlying knowledge obtained from old data sets is transferred to the new RNN models. Additionally, by training new RNN models with the most recent data set, the loss function in RNN learning algorithm is calculated based on the new data that captures nonlinear dynamics subject to recent disturbances only. Therefore, the updated RNN models are more capable of making accurate predictions accounting for recent disturbances. Moreover, the computation time for updating an RNN model is significantly reduced due to the small size of the newly collected data set compared to the original training data set. However, because of insufficient data in the new training data set, the updated RNN models are not guaranteed to approximate nonlinear dynamics subject to disturbances in the entire operating region. Therefore, RNN models will keep adapting to disturbances via the implementation of event-triggered and error-triggered mechanisms in this section, until they are accurate enough for LMPC and LEMPC to achieve closed-loop stability.

INTEGRATION OF ONLINE UPDATE OF RNNS WITH MPC

In this section, we demonstrate the implementation strategies for online updating RNN models in LMPC and LEMPC, respectively, following the event-triggering and error-triggering mechanisms introduced in the previous section. Subsequently, closed-loop stability is established for the nonlinear system of eq 1 subject to time-varying bounded disturbances under the sample-and-hold implementation of the LMPC of eq 9 and the LEMPC of eq 12, respectively.

Implementation Strategy for Online RNN Learning Within LMPC. On the basis of the event-triggered and error-triggered control schemes proposed in the previous sections, the implementation strategy (Figure 2) of the online RNN learning is integrated with the LMPC of eq 9 as follows:

1. An initial RNN model ensemble that is utilized in the LMPC of eq 9 is derived from extensive open-loop simulations for the nominal system of eq 1 (i.e., $w(t) \equiv 0$) following the construction method in ref 10.
2. Starting from an initial condition $x_0 \in \Omega_{\hat{\rho}} \backslash \Omega_{\rho_w}$, the nonlinear system of eq 1 is operated under LMPC in a sample-and-hold fashion with states being continuously monitored and collected. The update of RNN models is triggered the moment that eq 14 is violated and the optimal control actions $u^*(t)$ will be calculated by the LMPC using the new RNN model ensemble at the next sampling time.
3. Within finite sampling periods, the closed-loop state is driven into Ω_{ρ_w} under LMPC, after which we switch to the error-triggering mechanism as discussed in the section "Error-triggered Online RNN Update". Specifically, if the current state stays in Ω_{ρ_w}, the moving horizon error detector of eq 26 and its threshold E_T are utilized to determine whether an update of RNN models is in demand. However, if the current state leaves Ω_{ρ_w} due to disturbances, the event-triggering mechanism in *Step* 2 will be re-activated to trigger an RNN model update.
4. If the closed-loop state eventually enters a small neighborhood around the origin (i.e., $\Omega_{\rho_{min}}$ defined in eq 11), which is considered to be practically stable for the nominal system of eq 1, then both the event-triggering and the error-triggering mechanisms are taken off-line until the state leaves $\Omega_{\rho_{min}}$ again. Figure 1 shows a trajectory of a Lyapunov function under the LMPC with the above implementation strategy of on-line update of RNN models.

The following theorem is established to show that under the LMPC that incorporates the above implementation strategy of the event-triggered online update of RNN models, the closed-loop state of the nonlinear system of eq 1 is bounded in the stability region $\Omega_{\hat{\rho}}$ for all times, and ultimately enters Ω_{ρ_w}. Additionally, if the disturbances in the nonlinear system of eq 1 remain unchanged after some time, the closed-loop state can be ultimately bounded in a small neighborhood $\Omega_{\rho_{min}}$ around the origin.

Theorem 4. Consider the closed-loop system of eq 1 under the LMPC of eq 9 with the online update of the RNN models.

DOI: 10.1021/acs.iecr.9b03055
Ind. Eng. Chem. Res. 2020, 59, 2275−2290

Let $\Delta > 0$, $\varepsilon_w > 0$ and $\hat{\rho} > \rho_{\min} > \rho_s$ satisfy eq 10, eq 11, and eq 19. Then, given any initial state $x_0 \in \Omega_{\hat{\rho}}$, if the ensemble of RNN models is updated following the implementation strategy in this section with the triggering events of eq 14 and eq 27, then it is guaranteed that under the LMPC of eq 9, $x(t) \in \Omega_{\hat{\rho}}$, $\forall\, t \geq 0$, and $x(t)$ ultimately enters Ω_{ρ_w}. Additionally, if the disturbances $w(t)$ remain unchanged after $t = T_s > 0$, it holds that $\lim_{t \to \infty} \hat{V}(x(t)) \leq \rho_{\min}$ for the closed-loop system of eq 1.

Proof. We first prove that the state of the closed-loop system of eq 1 can be driven into Ω_{ρ_w} for any initial condition $x_0 \in \Omega_{\hat{\rho}} \backslash \Omega_{\rho_w}$. Since the RNN model is updated online following the condition in eq 14, the value of $\hat{V}(x(t))$ decreases at least at the rate of $-\varepsilon_w$ with respect to time if eq 14 is satisfied. However, in the case that an update of RNN models is triggered by the violation of eq 14 and the control actions remain unchanged until the next sampling step, it is shown in Proposition 2 that the state can still be driven to a smaller level set of $\hat{V}(x)$ within one sampling period. Therefore, it is guaranteed that the state ultimately converges to Ω_{ρ_w}. On the other hand, if $x(t_k) \in \Omega_{\rho_w}$, the online update of RNN models is subject to the error-triggering mechanism of eq 27. It is noted that the closed-loop state is not guaranteed to remain inside Ω_{ρ_w} for all times in the presence of bounded disturbances. However, once the state leaves Ω_{ρ_w}, it is shown by the characterization method of Ω_{ρ_w} that the state will not leave the closed-loop stability region $\Omega_{\hat{\rho}}$ within one sampling period, such that the state can be driven into Ω_{ρ_w} again under the LMPC of eq 9 with the event-triggering system of eq 14.

Next, we prove that after the disturbances $w(t)$ remain unchanged for all $t \geq T_s > 0$, the state of the closed-loop system of eq 1 is ultimately unbounded in $\Omega_{\rho_{\min}}$. Specifically, since $w(t) = w(T_s)$, $\forall\, t \geq T_s$, the last updated RNN models satisfy $|\nu| = |F(x, u, w(T_s)) - F_{nn}(x, u)| \leq \gamma|x|$. Therefore, based on eq 10, eq 11 and eq 23, the time-derivative of $\hat{V}(x)$, $\forall t \in [t_k, t_{k+1})$, where $t_k \geq T_s$, is bounded for all $x(t_k) \in \Omega_{\hat{\rho}} \backslash \Omega_{\rho_s}$ as follows:

$$\begin{aligned}\dot{\hat{V}}(x(t)) &\leq -\hat{c}_3|x(t_k)|^2 + \hat{c}_4\gamma|x(t_k)|^2 + L_x'|x(t) - x(t_k)| \\ &\quad + L_w'|w(t) - w(T_s)| \\ &\leq -\tilde{c}_3|x(t_k)|^2 + L_x'M\Delta \\ &\leq -\varepsilon_w \end{aligned} \tag{28}$$

This implies that well-conditioned RNN models are derived to successfully capture the dynamics of nonlinear system of eq 1 in the presence of constant disturbances $w(t)$ after $t = T_s$, and therefore, the closed-loop state can be ultimately driven into Ω_{ρ_s}. Following the definitions of $\Omega_{\rho_{nn}}$, $\Omega_{\rho_{\min}}$, and the proof in ref 10, it is demonstrated that the closed-loop state is maintained in a small neighborhood $\Omega_{\rho_{\min}}$ around the origin in the presence of sufficiently small modeling error $|\nu|$. This completes the proof of convergence of the state to Ω_{ρ_w} within a finite time, and boundedness of the state in $\Omega_{\hat{\rho}}$, $\forall t \geq 0$ for the closed-loop system of eq 1 with $x_0 \in \Omega_{\hat{\rho}}$ under the LMPC with the online update of RNN models.

Implementation Strategy for Online RNN Learning Within LEMPC. The integrated framework (Figure 2) of implementing online RNN learning within the LEMPC of eq 12 is presented as follows:

Algorithm

LMPC (Eq. 9):
1: Import initial RNN models into LMPC
2: **if** $x(t_k) \in \Omega_{\hat{\rho}} \backslash \Omega_{\rho_w}$:
activate event-triggered mechanism (Eq. 14)
elif $x(t_k) \in \Omega_{\rho_w} \backslash \Omega_{\rho_{min}}$:
activate error-triggered mechanism (Eq. 27)
else: stop updating RNN models
3: Update the RNN model if there is any in **Step 2**

LEMPC (Eq. 12):
1: Import initial RNN models into LEMPC
2: **if** $x(t_k) \in \Omega_{\hat{\rho}_e}$:
activate error-triggered mechanism (Eq. 27)
else : (i.e., $x(t_k) \in \Omega_{\hat{\rho}} \backslash \Omega_{\hat{\rho}_e}$)
activate event-triggered mechanism (Eq. 14)
3: Update the RNN model if there is any in **Step 2**

Figure 2. Algorithm of integrating online update of RNN models with LMPC and LEMPC.

Step 1. Similar to the implementation strategy for LMPC, an initial RNN model ensemble that is utilized in the LEMPC of eq 9 is derived from extensive open-loop simulations for the nominal system of eq 1 (i.e., $w(t) \equiv 0$) following the construction method in ref 14.

Step 2. Starting from an initial condition $x_0 \in \Omega_{\hat{\rho}}$, the nonlinear system of eq 1 is operated under LEMPC in a sample-and-hold fashion with states being continuously monitored and collected. Specifically, if $x(t_k) \in \Omega_{\hat{\rho}_e}$, the RNN models are updated following the error-triggered mechanism of eq 27. However, if $x(t_k) \in \Omega_{\hat{\rho}} \backslash \Omega_{\hat{\rho}_e}$, both the event-triggered mechanism of eq 14 and the error-triggered mechanism of eq 27 are activated, in which the update of RNN models is triggered by the one that violates the constraint first.

Step 3. Since the event-triggered mechanism of eq 14 is activated for all $x \in \Omega_{\hat{\rho}} \backslash \Omega_{\hat{\rho}_e}$, the closed-loop state is guaranteed to move into $\Omega_{\hat{\rho}_e}$ within finite sampling steps. Therefore, under the time-varying operation of LEMPC with online updating RNNs, optimal process economic benefits and closed-loop stability are achieved simultaneously for the closed-loop system of eq 1.

The following theorem demonstrates that under the LEMPC with online updating RNN models, the closed-loop state of the nonlinear system of eq 1 is maintained in the stability region $\Omega_{\hat{\rho}}$ for all times.

Theorem 5. Consider the closed-loop system of eq 1 under the LEMPC of eq 12 with the online update of the RNN models via the above implementation strategy. Let $\Delta > 0$, $\varepsilon_w > 0$ and $\hat{\rho} > \hat{\rho}_e > \rho_w > 0$ satisfy eq 10, eq 19, and the following inequality:

$$\hat{\rho}_e \leq \hat{\rho} - \frac{\hat{c}_4\sqrt{\hat{\rho}}}{\sqrt{\hat{c}_1}} f_w'(\Delta) - \kappa(f_w'(\Delta))^2 \tag{29}$$

where

DOI: 10.1021/acs.iecr.9b03055
Ind. Eng. Chem. Res. 2020, 59, 2275−2290

$$f_w'(t) := \frac{2L_w w_m + \nu_m}{L_x}(e^{L_x t} - 1)$$

Then, for any initial condition $x_0 \in \Omega_{\hat{\rho}}$, the closed-loop state $x(t)$ is bounded in the stability region $\Omega_{\hat{\rho}}$, $\forall t \geq 0$.

Proof. We prove the boundedness of state in $\Omega_{\hat{\rho}}$ for the following two cases: $x(t_k) \in \Omega_{\hat{\rho}_\epsilon}$ and $x(t_k) \in \Omega_{\hat{\rho}} \backslash \Omega_{\hat{\rho}_\epsilon}$. Specifically, we first prove that if $x(t_k) \in \Omega_{\hat{\rho}_\epsilon}$, the state of the nonlinear system of eq 1 subject to bounded disturbances does not leave $\Omega_{\hat{\rho}}$ within one sampling period (i.e., $\forall t \in [t_k, t_{k+1})$). Following the proof in refs 34 and 35, the time-derivative of the state error vector $e(t) = x(t) - \hat{x}(t)$ is obtained $\forall x, \hat{x} \in \Omega_{\hat{\rho}}$, $u \in U$, and $w(t) \in W$ as follows:

$$\begin{aligned} |\dot{e}| &= |F(x, u, w) - F_{nn}(\hat{x}, u)| \\ &\leq |F(x, u, w) - F(\hat{x}, u, w(r_k)| \\ &\quad + |F(\hat{x}, u, w(r_k)) - F_{nn}(\hat{x}, u)| \\ &\leq L_x|e(t)| + 2L_w w_m + \nu_m \end{aligned} \tag{30}$$

where it is assumed that the last updated RNN models are obtained at $t = r_k \leq t_k$. Because measured states are fed back to the controller at every sampling step, it follows that $x(t) = \hat{x}(t)$ (i.e., $e(0) = 0$). Thus, the upper bound for $|e(t)|$ is derived for all $x(t), \hat{x}(t) \in \Omega_{\hat{\rho}}$ and $|w(t)| \leq w_m$ as follows:

$$|e(t)| = |x(t) - \hat{x}(t)| \leq \frac{2L_w w_m + \nu_m}{L_x}(e^{L_x t} - 1) \tag{31}$$

Additionally, using the Taylor series expansion of $\hat{V}(x)$ around $\hat{x}$ and eq 7, the following inequality is derived $\forall x, \hat{x} \in \Omega_\rho$:

$$\begin{aligned} \hat{V}(x) &\leq \hat{V}(\hat{x}) + \frac{\partial \hat{V}(\hat{x})}{\partial x}|x - \hat{x}| + \kappa|x - \hat{x}|^2 \\ &\leq \hat{V}(\hat{x}) + \frac{\hat{c}_4\sqrt{\hat{\rho}}}{\sqrt{\hat{c}_1}}|x - \hat{x}| + \kappa|x - \hat{x}|^2 \end{aligned} \tag{32}$$

where $\kappa > 0$. Therefore, from eq 32, it is demonstrated that if $\Omega_{\hat{\rho}_\epsilon}$ is characterized to satisfy eq 29, the closed-loop state $x(t)$, $t \in [t_k, t_{k+1})$ is guaranteed to be bounded in $\Omega_{\hat{\rho}}$ since the predicted state $\hat{x}(t)$ is maintained inside $\Omega_{\hat{\rho}_\epsilon}$ by the constraint of eq 9e.

On the other hand, if $x(t_k) \in \Omega_{\hat{\rho}} \backslash \Omega_{\hat{\rho}_\epsilon}$, the constraint of eq 12f is activated such that the control action u decreases the value of $\hat{V}(\hat{x})$ based on the states predicted by the RNN model of eq 12b within the next sampling period. Additionally, under the coimplementation of event-triggered mechanisms of eq 14 and eq 27, it is ensured that the state of the closed-loop system of eq 1 satisfies $\hat{V}(x(t)) < \hat{V}(x(t_k))$, $\forall t \in (t_k, t_{k+1})$, and therefore, it never leaves $\Omega_{\hat{\rho}}$, and can be eventually driven back to $\Omega_{\hat{\rho}_\epsilon}$. This completes the proof of boundedness of the closed-loop state in $\Omega_{\hat{\rho}}$ for all $x_0 \in \Omega_{\hat{\rho}}$ under LEMPC.

Remark 9. As shown in Figure 2, the error-triggered and the event-triggered update of the RNN model are employed for both tracking MPC and economic MPC. Specifically, in tracking MPC, the event-triggered model update that is based on the decreasing rate of Lyapunov function value is first implemented to ensure that the closed-loop state is able to converge to a neighborhood around the origin under LMPC (i.e., Ω_{ρ_w}). For the state in Ω_{ρ_w}, the error-triggered model update is activated such that the state can be ultimately driven to the origin using the updated RNN models that capture the process dynamics accounting for disturbances. With regards to the implementation of the RNN model update in EMPC, the error-triggered mechanism is activated for any state in $\Omega_{\hat{\rho}_\epsilon}$, while the event-triggered model update works for the state in $\Omega_{\hat{\rho}} \backslash \Omega_{\hat{\rho}_\epsilon}$. Under the integration of the error-triggered and the event-triggered model updates, the desired closed-loop performance is achieved under EMPC in terms of guaranteed closed-loop stability (i.e., boundedness of state in $\Omega_{\hat{\rho}}$) and economic optimality.

Remark 10. The proposed online update of RNN models for MPC is not limited to processes/input spaces of low dimension. Given a nonlinear system with state dimension of n, and input dimension of m, the input to the RNN model is of dimension $m + n$, and the output is of dimension n. The computational complexity of training an RNN model is approximately linear to the size of input space, and the size of each hidden layer. The computation time is not an issue for the initial RNN model since it is trained off-line based on the entire data set. Additionally, when updating RNN models online, we only use the most recent data to update the RNN model instead of training a new RNN from the beginning. Therefore, the computation time is significantly reduced compared to that for the initial RNN model, and is less than one sampling period in our case. Moreover, parallel computing and hardware acceleration can be employed to further improve computational efficiency of training RNN models for large-scale systems.

APPLICATION TO A CHEMICAL PROCESS EXAMPLE

A chemical process example is used to illustrate the application of an online update of RNN models for LMPC and LEMPC, respectively. Specifically, a well-mixed, nonisothermal continuous stirred tank reactor (CSTR) in which an irreversible second-order exothermic reaction takes place is considered. The reaction transforms a reactant A to a product B ($A \rightarrow B$). The inlet concentration of A, the inlet temperature, and the feed volumetric flow rate of the reactor are C_{A0}, T_0, and F, respectively. The CSTR is equipped with a heating jacket that supplies/removes heat at a rate Q. The CSTR dynamic model is described by the following material and energy balance equations:

$$\frac{dC_A}{dt} = \frac{F}{V}(C_{A0} - C_A) - k_0 e^{-E/RT}C_A^2 \tag{33a}$$

$$\frac{dT}{dt} = \frac{F}{V}(T_0 - T) + \frac{-\Delta H}{\rho_L C_p}k_0 e^{-E/RT}C_A^2 + \frac{Q}{\rho_L C_p V} \tag{33b}$$

where C_A is the concentration of reactant A in the reactor, V is the volume of the reacting liquid in the reactor, T is the temperature of the reactor, and Q denotes the heat input rate. The concentration of reactant A in the feed is C_{A0}. The feed temperature and volumetric flow rate are T_0 and F, respectively. The reacting liquid has a constant density of ρ_L and a heat capacity of C_p. ΔH, k_0, E, and R represent the enthalpy of reaction, pre-exponential constant, activation energy, and ideal gas constant, respectively. Process parameter values are listed in Table 1.

We study the operation of the CSTR under LMPC and LEMPC with the same unstable steady-state (C_{As}, T_s) = (1.95 kmol/m^3,402 K), and (C_{A0_s} Q_s) = (4 kmol/m^3,0 kJ/h). The manipulated inputs are the inlet concentration of species A and the heat input rate, which are represented by the deviation

DOI: 10.1021/acs.iecr.9b03055
Ind. Eng. Chem. Res. 2020, 59, 2275−2290

Table 1. Parameter Values of the CSTR

$T_0 = 300$ K	$F = 5$ m^3/h
$V = 1$ m^3	$E = 5 \times 10^4$ kJ/kmol
$k_0 = 8.46 \times 10^6$ m^3/kmol h	$\Delta H = -1.15 \times 10^4$ kJ/kmol
$C_p = 0.231$ kJ/kg K	$R = 8.314$ kJ/kmol K
$\rho_L = 1000$ kg/m^3	$C_{A0_s} = 4$ kmol/m^3
$Q_s = 0.0$ kJ/h	$C_{A_s} = 1.22$ kmol/m^3
$T_s = 438$ K	

variables $\Delta C_{A0} = C_{A0} - C_{A0_s}$, $\Delta Q = Q - Q_s$, respectively. The manipulated inputs are bounded as follows: $|\Delta C_{A0}| \leq 3.5$ kmol/m^3 and $|\Delta Q| \leq 5 \times 10^5$ kJ/h. Therefore, the states and the inputs of the closed-loop system are $x^{\mathrm{T}} = [C_A - C_{As}\ T - T_s]$ and $u^{\mathrm{T}} = [\Delta C_{A0}\ \Delta Q]$, respectively, such that the equilibrium point of the system is at the origin of the state-space, (i.e., $(x_s^*, u_s^*) = (0,0)$). In this work, we consider the model variations caused by the following disturbances. (1) The feed flow rate F is varying due to an upstream disturbance that F becomes time-varying with the constraint: $0 \leq F \leq 12$ m^3/h. (2) Additionally, catalyst activation is accounted for during the operation of the CSTR of eq 33, which leads to a reduction in the reaction pre-exponential factor k_0 with the constraint: $0 < k_0 < 8.46 \times 10^6$ m^3/kmol h.

The control Lyapunov function $V(x) = x^{\mathrm{T}}Px$ is designed with the following positive definite P matrix:

$$P = \begin{bmatrix} 1060 & 22 \\ 22 & 0.52 \end{bmatrix} \tag{34}$$

Then, the closed-loop stability region Ω_ρ for the CSTR is characterized as a level set of the Lyapunov function with $\hat{\rho} = 368$ inside the region ϕ_w from which the origin can be rendered exponentially stable under the controller $u = \Phi(x) \in U$.

The explicit Euler method with an integration time step of $h_c = 10^{-4}$ h is used to numerically simulate the dynamic model of eq 33. The nonlinear optimization problem of the LMPC of eq 9 is solved using the python module of the IPOPT software package,[36] named PyIpopt with the sampling period $\Delta = 10^{-2}$ h. The initial ensemble of RNN models is generated following the data generation and RNN learning algorithm in refs 10 and 14. Parallel computing is employed to carry out the calculations of multiple RNN predictions concurrently using a Message Passing Interface (MPI) for the Python programming language, named *MPI4Py*.[37]

In this work, we assume that there is no noise in real-time data. However, in the case where the state measurements are noisy, the proposed online update of RNN models can still be applied via a data preprocessing step to smooth the measurement data. For example, Savitzky-Golay filter, a generalized moving average based on the least-squares fitting, can be applied to smooth noisy sampled data without distorting the data tendency before feeding real-time data into the RNN model.[38,39]

Remark 11. The matrix P in the Lyapunov function is derived via trial and error with an attempt to maximize the stability region (i.e., the largest level set Ω_ρ within the set of states in which $\dot{V}$ is rendered negative under the stabilizing controller $u = \Phi(x) \in U$). Different values of P will generate different set of states where $\dot{V} < 0$, and therefore, affect the size and the shape of the stability region.

Closed-Loop Simulation under LMPC. The control objective of LMPC is to operate the CSTR at the unstable equilibrium point (C_{As}, T_s) by manipulating the heat input rate ΔQ and the inlet concentration ΔC_{A0} under the LMPC using RNN models. The closed-loop simulation results for the nominal system of eq 33 under LMPC are shown in ref 10, where it is demonstrated that the state converges to a small neighborhood $\Omega_{\rho_{\min}}$ around the origin ultimately. The simulation results for the uncertain system of eq 33 under LMPC with an online update of the RNN model ensemble are shown in Figures 3−9. Specifically, the feed flow rate F is increased to 12 m^3/h at t = 0.05 h, and k_0 is gradually decreased to $0.8k_0$, $0.6k_0$, and $0.4k_0$ at t = 0.1, 0.2, and 0.4 h, respectively, and remains unchanged afterward. In Figure 3, it is shown that the closed-loop state trajectory under LMPC without the online update of the RNN model ensemble (i.e., using the initial RNN model ensemble for all times) oscillates around the origin due to disturbances, while the LMPC with the online update of the RNN model ensemble successfully drives the closed-loop state into a small neighborhood around the origin. Additionally, in Figure 4 and Figure 5, it is shown that the closed-loop states under the LMPC with the online RNN update are stabilized at their steady-states after t = 0.2 h, while those under the LMPC without the online RNN update show considerable oscillation since the initial RNN model ensemble is not able to capture the dynamic behavior of the system of eq 33 in the presence of disturbances. Therefore, the dynamic performance of the closed-loop system of eq 33 under the LMPC is significantly improved through the online update of the RNN model ensemble.

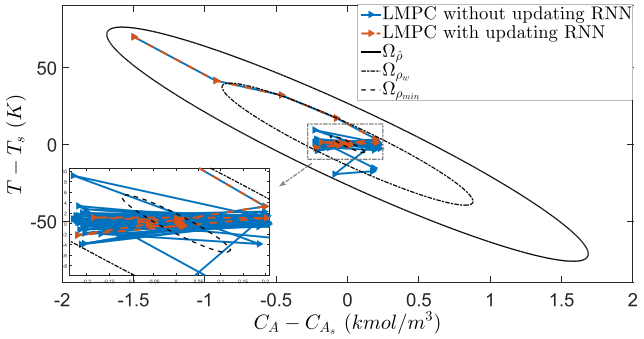

Figure 3. State-space profiles for the closed-loop CSTR under the LMPC of eq 9 with and without the online update of the RNN model ensemble for the initial condition (−1.5, 70).

Figure 6 shows the evolution of the moving horizon error detector $E_{\mathrm{rnn}}(t)$ for the closed-loop system of eq 33 under the LMPC of eq 9 with the error-triggered online update of the RNN models. Specifically, since it takes only one sampling step for the closed-loop state to enter Ω_{ρ_w}, the event-triggering condition of eq 14 is never triggered in this case. Additionally, in Figure 6, it is shown that the update of the RNN models is triggered two times with the threshold $E_T = 15$. After the closed-loop state enters a small neighborhood around the origin (i.e., $\Omega_{\rho_{\min}}$), the error-triggering system is off-line according to the implementation strategy (i.e., Step 4) for LMPC.

Figure 7 depicts the evolution of the Lyapunov function value, $\hat{V}(x)$, of the closed-loop state, under the LMPC with and without the online update of the RNN models, respectively. In Figure 7, the closed-loop state under the online update enters $\Omega_{\rho_{\min}}$ after t = 0.1 h in the presence of disturbances, while it oscillates heavily and never enters $\Omega_{\rho_{\min}}$ under the LMPC without online model update. Finally, in Figure 8 and Figure 9, the manipulated input profiles for $u_1 = \Delta C_{A0}$ and $u_2 = \Delta Q$ are

DOI: 10.1021/acs.iecr.9b03055
Ind. Eng. Chem. Res. 2020, 59, 2275−2290

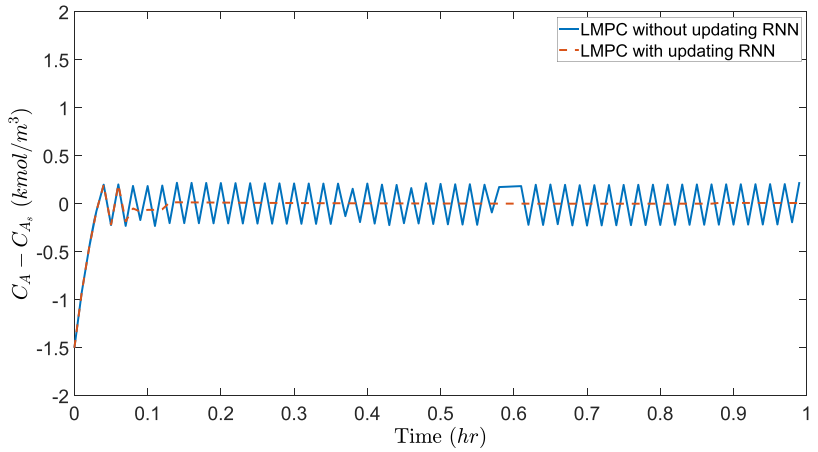

Figure 4. State profiles $(x_1 = C_A - C_{As})$ for the initial condition $(-1.5, 70)$ under the LMPC of eq 9 with and without the online update of the RNN model ensemble, respectively.

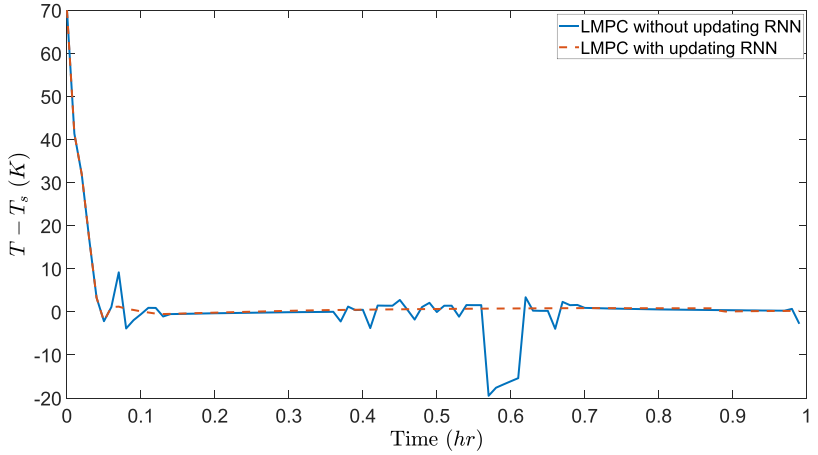

Figure 5. State profiles $(x_2 = T - T_s)$ for the initial condition $(-1.5, 70)$ under the LMPC of eq 9 with and without the online update of the RNN model ensemble, respectively.

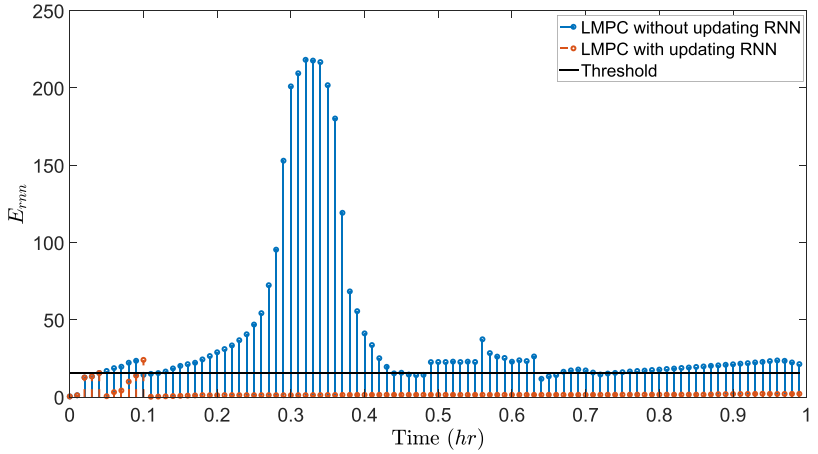

Figure 6. Value of $E_{\text{rnn}}(t)$ of eq 26 at each sampling time for the closed-loop system of eq 33 under the LMPC of eq 9 with error-triggered online update of RNN models.

presented for both LMPCs. Specifically, when the RNN models are updated online, u_1 in Figure 8 settles to its steady-state value after $t = 0.12$ h. However, without the online update of the RNN models, u_1 shows sustained oscillation between the maximum and minimum saturated points, which might significantly shorten the lifespan of the actuators. Similarly, in Figure 9, the LMPC with the online update of the RNN models shows smoother control actions u_2 compared to that without the online model update.

Closed-Loop Simulation under LEMPC. The control objective of LEMPC is to maximize the profit of the CSTR process of eq 33 by manipulating the inlet concentration ΔC_{A0}

DOI: 10.1021/acs.iecr.9b03055
Ind. Eng. Chem. Res. 2020, 59, 2275−2290

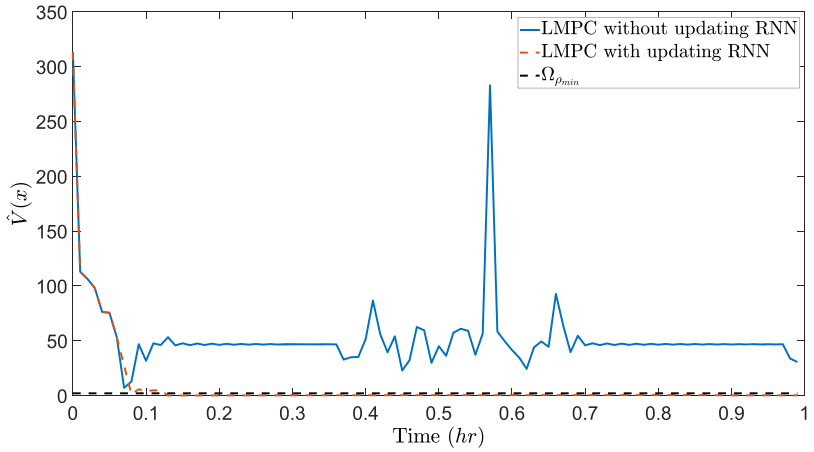

Figure 7. Evolution of $\hat{V}(x)$ for the closed-loop system of eq 33 under the LMPC of eq 9 with and without the error-triggered online update of RNN models.

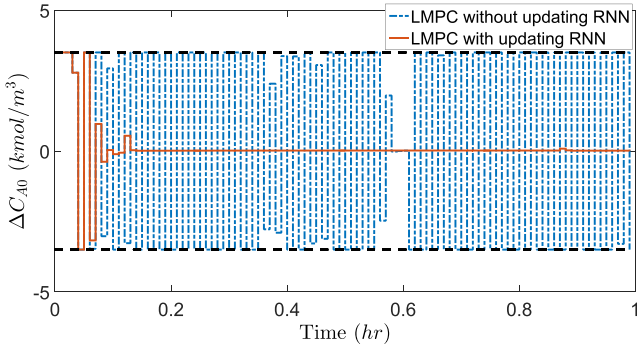

Figure 8. Manipulated input profiles ($u_1 = \Delta C_{A0}$) for the initial condition (−1.5, 70) under the LMPC of eq 9 with and without the online update of the RNN model ensemble, respectively, where the black dotted lines represent the upper and lower bound for u_1.

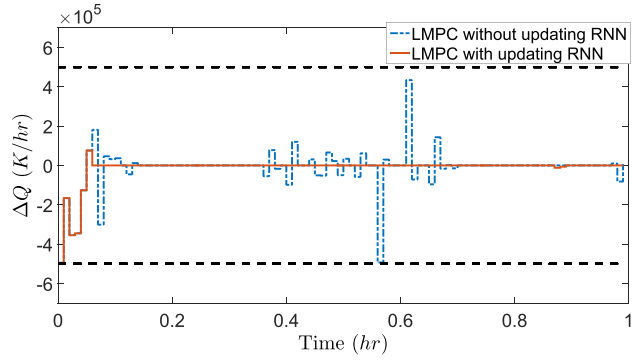

Figure 9. Manipulated input profiles ($u_2 = \Delta Q$) for the initial condition (−1.5, 70) under the LMPC of eq 9 with and without the online update of the RNN model ensemble, respectively, where the black dotted lines represent the upper and lower bound for u_2.

and the heat input rate ΔQ, and meanwhile maintain the closed-loop state trajectories in the stability region $\Omega_{\hat{\rho}}$ for all times under LEMPC. The objective function of the LEMPC optimizes the production rate of B as follows:

$$l_e(\tilde{x}, u) = k_0 \, e^{-E/RT} C_A^2 \tag{35}$$

Additionally, the following material constraint is utilized in the LEMPC of eq 12 to make the averaged reactant material available within the operating period t_p to be its steady-state value, C_{A0s} (i.e., the averaged reactant material in deviation form, u_1, is equal to 0).

$$\frac{1}{t_p}\int_0^{t_p} u_1(\tau)\, d\tau = 0 \quad \text{kmol/m}^3 \tag{36}$$

In ref 14 it has been demonstrated that the closed-loop state of the nominal system of eq 33 is bounded in $\Omega_{\hat{\rho}}$ for all times under LEMPC. In this work, we consider the same disturbances that we have performed for the closed-loop system of eq 33 under LMPC. Additionally, the CSTR system of eq 33 is operated under LEMPC for five consecutive operation periods with t_p = 0.2 h for each operation period. The simulations results for the closed-loop system of eq 33 in the presence of disturbances are shown in Figures 10−16. Specifically, in Figure 10, it is shown

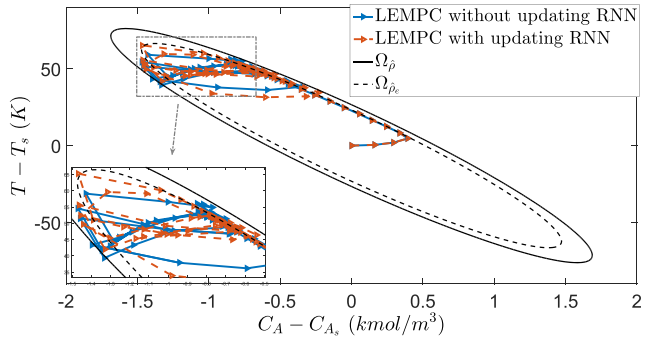

Figure 10. State trajectories for the closed-loop CSTR under the LEMPC of eq 12 with and without the online update of the RNN model ensemble for the initial condition (0, 0).

that the closed-loop state circles inside the stability region $\Omega_{\hat{\rho}}$ due to the time-varying operation under LEMPC. Additionally, it is demonstrated that the closed-loop state is bounded in $\Omega_{\hat{\rho}}$ for all times under the LEMPC of eq 12 with the online update of the RNN models. From Figure 11, it is shown that the moving horizon error detector E_{rnn} exceeds the threshold twice under the LEMPC with the online update of the RNN models (i.e., the RNN update is triggered twice), and ultimately remains at a low value (below the threshold) after a more accurate ensemble of RNN models are derived to account for process disturbances. However, it is observed that the error detector E_{rnn} under the LEMPC without the online update of the RNN models maintains at a high level (close to the threshold) for all times,

DOI: 10.1021/acs.iecr.9b03055
Ind. Eng. Chem. Res. 2020, 59, 2275−2290

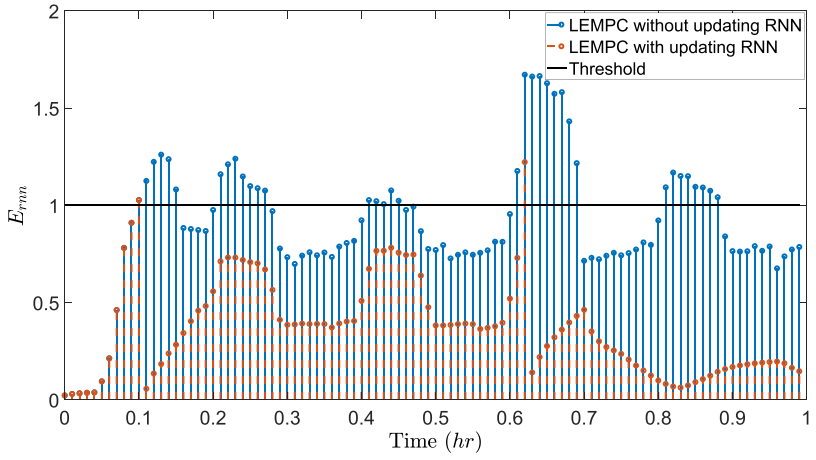

Figure 11. Value of $E_{\text{rnn}}(t)$ of eq 26 at each sampling time for the closed-loop system of eq 33 under the LEMPC of eq 12 with the error-triggered online update of the RNN models.

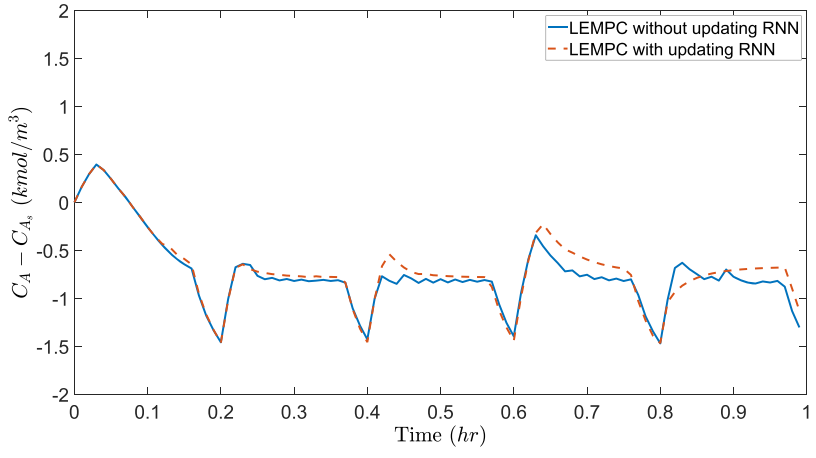

Figure 12. State profiles ($x_1 = C_A - C_{As}$) for the initial condition $(0, 0)$ under the LEMPC of eq 12 with and without the online update of the RNN model ensemble, respectively.

which implies that the deviation between the predicted state and the actual states is considerable, and may lead to undesired closed-loop performance. Moreover, it is observed in Figure 14 that the event-triggered mechanism of eq 14 is never activated in this case since $\hat{V}(x)$ decreases rapidly for all states outside $\Omega_{\hat{\rho}_e}$, and thus, satisfies $\hat{V}(x(t)) \leq \hat{V}(x(t_k)) - \varepsilon_w(t - t_k)$, $t \in [t_k, t_{k+1})$.

On the basis of the state profiles shown in Figure 12 and Figure 13, the evolution of the value of $\hat{V}(x)$ for the closed-loop system of eq 33 is compared between the LEMPC with and without the online update of the RNN models in Figure 14. Specifically, it is shown that $\hat{V}(x)$ under LEMPC with the online update of the RNN models remains below 368 (i.e., the value of $\hat{\rho}$ for the closed-loop stability region $\Omega_{\hat{\rho}}$) for all times, while it exceeds 368 under the LEMPC without the online update of the RNN models around $t = 0.2$ h and $t = 0.6$ h. Additionally, since the accuracy of the RNN prediction for nonlinear dynamics of eq 33 subject to disturbances is improved via the online update using real-time process data, $\hat{V}(x)$ is smoothly maintained below $\hat{\rho}_e$ during the last 0.4 h. However, $\hat{V}(x)$ based on the states under the LEMPC without the online update of the RNN models shows sustained oscillation around $\hat{\rho}_e$ due to significant model mismatch as indicated in Figure 11.

Manipulated input profiles for the closed-loop system of eq 33 are given in Figure 15 and Figure 16, in which it is shown that the input constraints on ΔC_{A0} and ΔQ are satisfied for all times.

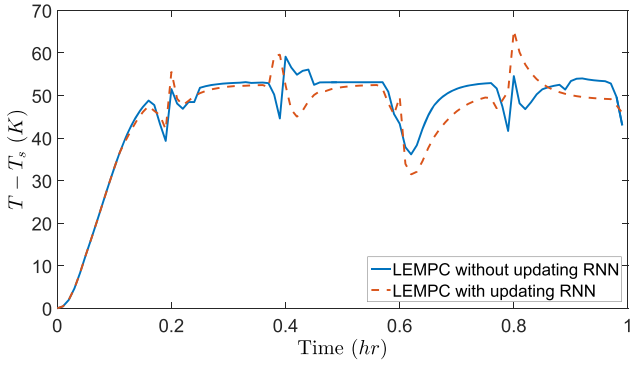

Figure 13. State profiles ($x_2 = T - T_s$) for the initial condition $(0, 0)$ under the LEMPC of eq 12 with and without the online update of the RNN model ensemble, respectively.

Additionally, it is observed in Figure 15 that the closed-loop system initially consumes the maximum allowable ΔC_{A0} (i.e., $\Delta C_{A0} = 3.5\text{kmol/m}^3$) within each operation period ($t_p = 0.2$ h) to maximize the production rate of B, and therefore, has to lower the reactant consumption near the end of each operation period to meet the material constraint of eq 36 for all times.

Lastly, the total economic benefits achieved within five operation periods are calculated for the LEMPC with the online

DOI: 10.1021/acs.iecr.9b03055
Ind. Eng. Chem. Res. 2020, 59, 2275−2290

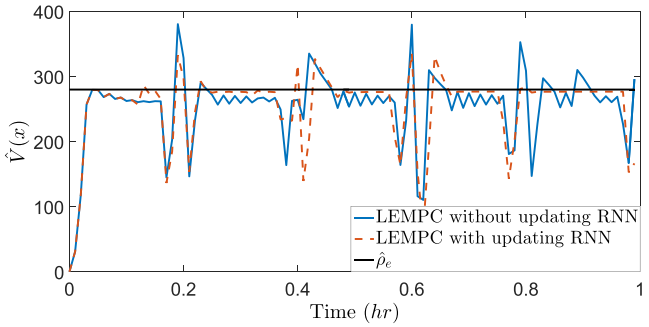

Figure 14. Evolution of $\hat{V}(x)$ for the closed-loop system of eq 33 under the LEMPC of eq 12 with and without the error-triggered online update of the RNN models, respectively.

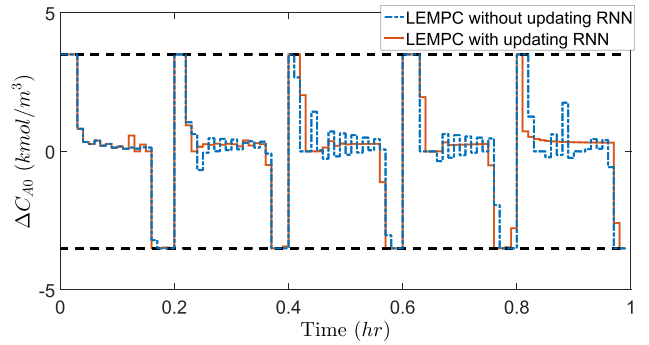

Figure 15. Manipulated input profiles ($u_1 = \Delta C_{A0}$) for the initial condition (0, 0) under the LEMPC of eq 12 with and without the online update of the RNN model ensemble, respectively, where the black dotted lines represent the upper and lower bounds for u_1.

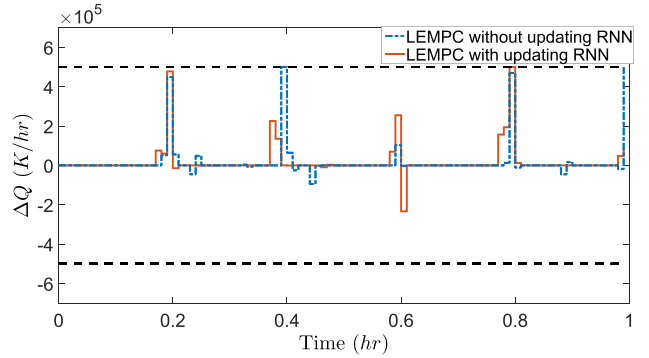

Figure 16. Manipulated input profiles ($u_2 = \Delta Q$) for the initial condition (0, 0) under the LEMPC of eq 12 with and without online update of RNN model ensemble, respectively, where the black dotted lines represent the upper and lower bounds for u_2.

update of the RNN models and the steady-state operation (i.e., the system of eq 33 is operated at (C_{As}, T_s) for all times) using the following equation

$$L_E = \int_0^{St_p} l_e(x, u)\, dt$$

It is shown that L_E = 16.74 for the closed-loop system under LEMPC and L_E = 10.23 for the steady-state operation within 1 h. Therefore, it is concluded that time-varying operation of the system of eq 33 under the LEMPC of eq 12 with the online updating RNN models achieves higher economic benefits compared to the steady-state operation, and outperforms that without the online update of RNN models in terms of smoother operation and stronger properties of robustness.

Remark 12. The averaged computation time for solving the LMPC optimization problem without the online update of the RNN models at each sampling step is around 11 s, which is less than one sampling period (i.e., Δ = 0.01 h = 36 s), while the averaged computation time for solving the LEMPC optimization problem without the online model update is less than 8 s. Additionally, the computation time for online training/updating an RNN model within LMPC/LEMPC is around 15 s.

Remark 13. The quasi-periodicity of closed-loop state and input profiles is due to the reactant material constraint that is incorporated in LEMPC. Since it is required that the averaged reactant material used within each operating period is equal to its steady-state value (i.e., reactant material constraint), LEMPC consumes the maximum allowable reactants and energy at the early stage of each operating period (owing to the second-order reaction rate to maximize reaction rate), and lowers the reactant consumption near the end of the period to meet the material constraint. In the simulation, the CSTR system is operated under LEMPC for five operating periods, and therefore, the state and input profiles exhibit quasi-periodic behavior.

CONCLUSION

This work focused on the real-time implementation of machine learning-based MPC and EMPC to nonlinear processes subject to time-varying disturbances. On the basis of the ensemble of RNN models that were obtained from extensive simulation data, Lyapunov-based MPC was developed to drive the state of the nominal closed-loop system to the steady-state, and Lyapunov-based EMPC was developed to maintain the state in the closed-loop stability region, respectively. Subsequently, event-triggered and error-triggered mechanisms were incorporated in LMPC and LEMPC to update the RNN models online using the most recent process data that account for nonlinear dynamics in the presence of disturbances. The application of the proposed methodology to a chemical process example demonstrated that the closed-loop state converged to the origin under LMPC, and remained bounded in the closed-loop stability region under LEMPC with improved dynamic performance compared to those without the online update of the RNN models.

AUTHOR INFORMATION

Corresponding Author

*E-mail: pdc@seas.ucla.edu.

ORCID

Panagiotis D. Christofides: 0000-0002-8772-4348

Notes

The authors declare no competing financial interest.

REFERENCES

(1) Ge, S. S.; Wang, C. Adaptive neural control of uncertain MIMO nonlinear systems. *IEEE Transactions on Neural Networks* **2004**, *15*, 674−692.

(2) Ge, H. W.; Liang, Y. C.; Marchese, M. A modified particle swarm optimization-based dynamic recurrent neural network for identifying and controlling nonlinear systems. *Comput. Struct.* **2007**, *85*, 1611−1622.

(3) Chow, T. W.; Fang, Y. A recurrent neural-network-based real-time learning control strategy applying to nonlinear systems with unknown dynamics. *IEEE Transactions on Industrial Electronics* **1998**, *45*, 151−161.

DOI: 10.1021/acs.iecr.9b03055
Ind. Eng. Chem. Res. 2020, 59, 2275−2290

(4) Chen, V. C. P.; Rollins, D. K. Issues regarding artificial neural network modeling for reactors and fermenters. *Bioprocess Eng.* **2000**, *22*, 85−93.
(5) Himmelblau, D. M. Applications of artificial neural networks in chemical engineering. *Korean J. Chem. Eng.* **2000**, *17*, 373−392.
(6) Hernández, E.; Arkun, Y. Study of the control-relevant properties of backpropagation neural network models of nonlinear dynamical systems. *Comput. Chem. Eng.* **1992**, *16*, 227−240.
(7) Chaffart, D.; Ricardez-Sandoval, L. A. Optimization and control of a thin film growth process: A hybrid first principles/artificial neural network based multiscale modelling approach. *Comput. Chem. Eng.* **2018**, *119*, 465−479.
(8) Mohanty, S. Artificial neural network based system identification and model predictive control of a flotation column. *J. Process Control* **2009**, *19*, 991−999.
(9) Gençay, R.; Liu, T. Nonlinear modelling and prediction with feedforward and recurrent networks. *Phys. D* **1997**, *108*, 119−134.
(10) Wu, Z.; Tran, A.; Rincon, D.; Christofides, P. D. Machine Learning-Based Predictive Control of Nonlinear Processes. Part I: Theory. *AIChE J.* **2019**, *65*, e16729 DOI: 10.1002/aic.16729.
(11) Wu, Z.; Tran, A.; Rincon, D.; Christofides, P. D. Machine Learning-Based Predictive Control of Nonlinear Processes. Part II: Computational Implementation. *AIChE J.* **2019**, *65*, e16734 DOI: 10.1002/aic.16734.
(12) Durand, H.; Christofides, P. D. Actuator stiction compensation via model predictive control for nonlinear processes. *AIChE J.* **2016**, *62*, 2004−2023.
(13) Durand, H.; Christofides, P. D. Economic Model Predictive Control: Handling Valve Actuator Dynamics and Process equipment Considerations. *Foundations and Trends in Systems and Control* **2018**, *5*, 293−350.
(14) Wu, Z.; Christofides, P. D. Economic Machine-Learning-Based Predictive Control of Nonlinear Systems. *Mathematics* **2019**, *7* (6), 494.
(15) Valappil, J.; Georgakis, C. Systematic estimation of state noise statistics for extended Kalman filters. *AIChE J.* **2000**, *46*, 292−308.
(16) Marquardt, W. Nonlinear model reduction for optimization based control of transient chemical processes. *Proceedings of CPC VI*; AIChE Symposium Series; AIChE, 2002.
(17) Ge, S. S.; Hang, C. C.; Zhang, T. Stable adaptive control for nonlinear multivariable systems with a triangular control structure. *IEEE Trans. Autom. Control* **2000**, *45*, 1221−1225.
(18) Lin, F. J.; Lee, T. S.; Lin, C. H. Robust H_∞ controller design with recurrent neural network for linear synchronous motor drive. *IEEE Transactions on Industrial Electronics* **2003**, *50*, 456−470.
(19) Rasoulian, S.; Ricardez-Sandoval, L. A. Robust multivariable estimation and control in an epitaxial thin film growth process under uncertainty. *J. Process Control* **2015**, *34*, 70−81.
(20) Nagy, Z. K.; Braatz, R. D. Distributional uncertainty analysis using power series and polynomial chaos expansions. *J. Process Control* **2007**, *17*, 229−240.
(21) Rasoulian, S.; Ricardez-Sandoval, L. A. Stochastic nonlinear model predictive control applied to a thin film deposition process under uncertainty. *Chem. Eng. Sci.* **2016**, *140*, 90−103.
(22) Chaffart, D.; Ricardez-Sandoval, L. A Robust optimization of a multiscale heterogeneous catalytic reactor system with spatially-varying uncertainty descriptions using polynomial chaos expansions. *Can. J. Chem. Eng.* **2018**, *96*, 113.
(23) Choy, M. C.; Srinivasan, D.; Cheu, R. L Neural networks for continuous online learning and control. *IEEE Transactions on Neural Networks* **2006**, *17*, 1511−1531.
(24) Alanqar, A.; Durand, H.; Christofides, P. D. Error-triggered on-line model identification for model-based feedback control. *AIChE J.* **2017**, *63*, 949−966.
(25) Tabuada, P. Event-triggered real-time scheduling of stabilizing control tasks. *IEEE Trans. Autom. Control* **2007**, *52*, 1680−1685.
(26) Wang, X.; Lemmon, M. D. Event design in event-triggered feedback control systems. *Proc. 47th IEEE Conf. Decision Control* **2008**, 2105−2110.
(27) Wu, Z.; Jia, Q. S.; Guan, X. Optimal control of multiroom HVAC system: An event-based approach. *IEEE Transactions on Control Systems Technology* **2015**, *24*, 662−669.
(28) Sahoo, A.; Xu, H.; Jagannathan, S. Neural network-based event-triggered state feedback control of nonlinear continuous-time systems. *IEEE Transactions on Neural Networks and Learning Systems* **2016**, *27*, 497−509.
(29) Liu, D.; Yang, G. H. Neural network-based event-triggered MFAC for nonlinear discrete-time processes. *Neurocomputing* **2018**, *272*, 356−364.
(30) Khalil, H. K. *Nonlinear systems*; Prentice Hall: Upper Saddle River, NJ, 2002; Vol. *3*.
(31) Lin, Y.; Sontag, E. D. A universal formula for stabilization with bounded controls. *Systems and Control Letters* **1991**, *16*, 393−397.
(32) Rawlings, J. B.; Maravelias, C. T. Bringing new technologies and approaches to the operation and control of chemical process systems. *AIChE J.* **2019**, *65*, e16615.
(33) Heemels, W.; Johansson, K. H.; Tabuada, P. An introduction to event-triggered and selftriggered control. *Proce. 51st IEEE Conf. Decision Control* **2012**, 3270−3285.
(34) Alanqar, A.; Ellis, M.; Christofides, P. D. Economic model predictive control of nonlinear process systems using empirical models. *AIChE J.* **2015**, *61*, 816−830.
(35) Wu, Z.; Durand, H.; Christofides, P. D. Safe economic model predictive control of nonlinear systems. *Systems and Control Letters* **2018**, *118*, 69−76.
(36) Wächter, A.; Biegler, L. T. On the implementation of an interior-point filter line-search algorithm for large-scale nonlinear programming. *Mathematical Programming* **2006**, *106*, 25−57.
(37) Dalcin, L. D.; Paz, R. R.; Kler, P. A.; Cosimo, A. Parallel distributed computing using Python. *Adv. Water Resour.* **2011**, *34*, 1124−1139.
(38) Ni, W.; Tan, S. K.; Ng, W. J.; Brown, S. D. Moving-window GPR for nonlinear dynamic system modeling with dual updating and dual preprocessing. *Ind. Eng. Chem. Res.* **2012**, *51*, 6416−6428.
(39) Rhode, S.; Hong, S.; Hedrick, J. K.; Gauterin, F. Vehicle tractive force prediction with robust and windup-stable Kalman filters. *Control Engineering Practice* **2016**, *46*, 37−50.

DOI: 10.1021/acs.iecr.9b03055
Ind. Eng. Chem. Res. 2020, 59, 2275−2290